Computational Models for Fracture and Degradation of Structures

Session Organizers: Günther MESCHKE (Ruhr University Bochum), Jan ROTS (TU-Delft**)**

Stepwise softening for concrete and masonry structures
Jan G. ROTS, Max A.N. HENDRIKS, Matt J. DEJONG (TU-Delft), Beatrice BELLETTI (University of Parma)*

The multi-scale approach of masonry, paradigm of the clay brick
Konrad J. KRAKOWIAK, Paulo B. LOURENÇO (University of Minho), Franz-J. ULM (MIT)*

Simplified modeling strategies for non linear dynamic calculations of RC structural walls including soil-structure interaction
Panagiotis KOTRONIS, J. MAZARS, S. GRANGE, C. GIRY (Grenoble Universités)*

Modeling mixed-mode crack propagation in reinforced concrete
Rena C. YU, Gonzalo RUIZ, Jacinto R. CARMONA (University of Castilla-La Mancha)*

Limit-analysis based identification of fracture and degradation mechanisms in two-phase composite materials
Josef FÜSSL (TU Vienna), Roman LACKNER (TU Munich)*

Fracture analyses of fiber-reinforced concrete structures
John BOLANDER (University of California, Davis)

Crack-centered enrichment for debonding in two-phase composite applied to textile reinforced concrete
Rostislav CHUDOBA, Jakub JEŘÁBEK, Frank PEIFFER, Joseph HEGGER (RWTH Aachen)*

Three-dimensional higher order X-FEM model for multifield durability and failure analysis of concrete structures
Stefan JOX, Christian BECKER, Günther MESCHKE (Ruhr University Bochum)*

From multi-scale to multi-grid FE analysis of concrete fracture
Chris J. PEARCE, Łukasz KACZMARCZYK, Nenad BIĆANIĆ (University of Glasgow)*

Analysis of thin layer ductile concrete as a seismic retrofit for masonry infill walls
Marios A. KYRIAKIDES, Sarah L. BILLINGTON (Stanford University)*

Mesoscopic failure simulation of concrete and life-cycle computation of concrete structures
Kohei NAGAI, Koich MAEKAWA (University of Tokyo)*

For multiple-author papers:
Contact author designated by *
Presenting author designated by underscore

Proceedings of the 6th International Conference on
Computation of Shell and Spatial Structures
IASS-IACM 2008: "Spanning Nano to Mega"
28-31 May 2008, Cornell University, Ithaca, NY, USA
John F. ABEL and J. Robert COOKE (eds.)

Stepwise softening for concrete and masonry structures

Jan G. ROTS*, Max A.N. HENDRIKS, Matt J. DEJONG, Beatrice BELLETTI

*Faculty of Civil Engineering and Geosciences & Faculty of Architecture
TU Delft, PO Box 5048, 2600 GA Delft, The Netherlands
j.g.rots@tudelft.nl

Abstract

Softening problems at structural level involve snap-backs and bifurcations, leading to difficulties with negative tangent stiffness in Newton-Raphson incremental-iterative schemes. This paper presents an alternative: a sequentially linear saw-tooth softening model. Instead of a single nonlinear analysis, a series of scaled linear analyses is performed keeping memory of local strength and stiffness reduction. The softening diagram of negative slope is replaced by a saw-tooth diagram of positive slopes. First, the method is reviewed. Next, recent progress and two extensions are described. The first relates to a generic ripple model for softening in tension and compression, as well as reinforcement plasticity. The second extension is a scaling technique for non-proportional loadings. Structural examples are included, showing the robustness of the approach.

1. Introduction

Cracks in concrete and large-scale masonry structures occur in a discontinuous manner, both discontinuous in space and discontinuous in time. This paper addresses the discontinuity in time, with the loading process. The crack development during loading involves stress redistributions accompanied by peaks, valleys, snap-backs and subsequent recoveries in the load-displacement response.

Numerically speaking, this jumpy and spiky response is difficult to trace. The incremental-iterative Newton-Raphson scheme for the nonlinear analysis may fail. A reason is that we use softening stress-strain relations of negative slope, involving negative stiffness. Also, the Newton-Raphson scheme has been meant originally for "smooth" problems, but seems to be less suited for problems with peaks, snaps and jumps. Remedies like arc-length techniques help, but cannot stabilize all cases.

This paper presents an alternative method: a sequentially linear saw-tooth softening model. Instead of a single nonlinear analysis, a series of linear analyses is performed keeping memory of local stiffness reduction. The softening curve of negative slope is replaced by a saw-tooth diagram of positive slopes. The incremental-iterative procedure is replaced by a scaled sequentially linear procedure. Advantages of this stepwise softening model are robustness, automatic detection of peaks and snap-backs and avoidance of bifurcations, while regular (dis)continuum notions like principal stress, strength, fracture energy and mesh size objectivity are preserved. The approach fits engineer's thinking. RC practitioners globally reduce concrete stiffness at areas of anticipated cracking. The present approach does the same, but then locally and automatically, at finite element level.

The paper includes recent extensions of the model to new saw-tooth shapes and to non-proportional loading.

2. Overall procedure of the model

The locally brittle snap-type response of RC and masonry structures inspired the idea to capture these brittle events directly rather than trying to iterate around them in a Newton-Raphson scheme (Rots and Invernizzi [1]). A critical "event" is traced and subsequently a secant restart is made from the origin for tracing the next critical event. Hence, the procedure is sequential rather than incremental. The sequence of critical events governs the load-displacement response. To this aim, the softening diagram is replaced by a saw-tooth curve and linear analyses are carried out sequentially. The global procedure is as follows. The structure is discretized using

standard elastic continuum elements. Young's modulus, Poisson's ratio and initial strength are assigned to the elements. Subsequently, the following steps are carried out sequentially:

- Add the external load as a unit load.
- Perform a linear elastic analysis.
- Extract the 'critical element' from the results. The 'critical element' is the element for which the stress level divided by its current strength is the highest in the entire structure, in other words, the element that is closest to its current saw-tooth peak.
- Calculate the ratio between the strength and the stress level in the critical element: this ratio provides the 'global load factor'. The present solution step is obtained rescaling the 'unit load elastic solution' times the 'global load factor'.
- Increase the damage in the critical element by reducing its stiffness and strength, i.e. Young's modulus E and tensile strength f_t, according to a saw-tooth diagram. This corresponds to a local damage "event".
- Repeat the previous steps for the new configuration, i.e. re-run a linear analysis for the structure in which E and f_t of the previous critical element have been reduced. Trace the next critical saw-tooth in some element, repeat this process till the damage has spread into the structure to the desired level.

Different philosophies can be posed to interpret the model. One interpretation is that the procedure jumps from event to event. Only one breakage or reduction occurs at a time, and then the next event is traced. This differs from other models, where multiple integration points may crack, crush or yield simultaneously in one step, involving bifurcations and survival aspects. A second interpretation is that the softening is discretized. Usually, researchers discretize the space into finite elements and discretize the load into load steps, and then search for associated material states along a continuous stress-strain diagram. Here, we rather discretize the softening into a limited number of possible material states (the saw-teeth), we discretize the space into finite elements, and then recompute the load belonging to that. A third interpretation is that the model does not involve load control, neither does it involve (direct or indirect) displacement control, but it represents damage control. A damage increment (reduction of local stiffness and strength at integration point) is specified rather than a load or displacement increment.

3. Saw-tooth approximations

The way in which the stiffness and strength of the critical elements are progressively reduced at each "event" constitutes the essence of the model. Different saw-tooth approaches are summarized in Fig. 1.

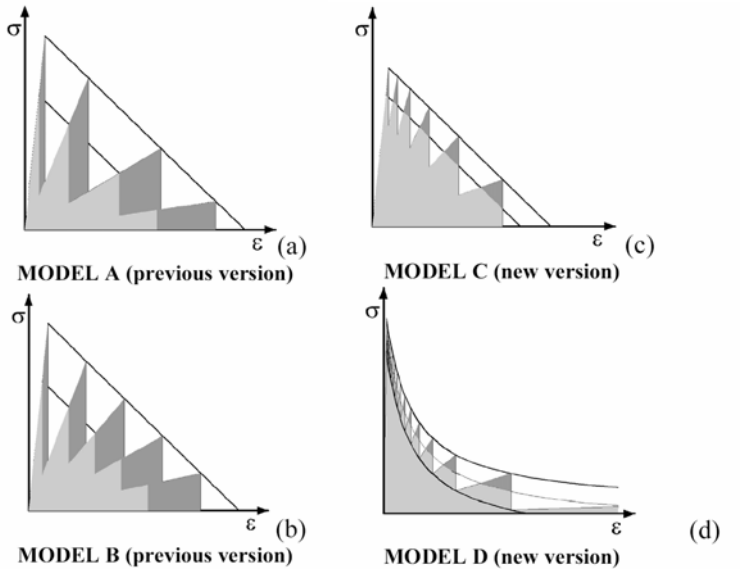

Figure 1: Saw-tooth approximations of softening stress-strain diagrams.

All diagrams are based upon tensile softening, defined by Young's modulus E, the tensile strength f_t, the shape of the diagram, and the area under the diagram. The area under the diagram represents the fracture energy G_f divided by the crack band width h, which is a discretization parameter associated with the size, orientation and integration scheme of the finite element. The softening diagram is adopted as a 'mother' or envelope curve that determines the consecutive strength reduction in sequentially linear analysis.

Model A starts from a step-wise reduction of Young's modulus by a certain constant factor a, to be set by the user. As an example, for a=2, E is consecutively reduced to E/2, E/4, E/8, E/16 etc. The reduction of the strength then results from the assumption for the shape of the softening diagram and the area under the softening diagram. Although this model served fairly well, it sometimes gave a sharp drop in the beginning, or it ended up with inaccurate approximations at the end of softening diagram. Also, the choice for the factor a was not trivial.

Model B starts from a stepwise reduction of the strength in equidistant portions. As an example, f_t can be consecutively reduced to e.g. 90% of its original value, 80%, 70% etc. The corresponding stepwise reduction of Young's modulus E is then recalculated from the shape of the softening diagram and the area underneath. This model appeared to perform better near the tail, but it often showed a too sharp drop in the beginning, also visible in Fig. 1b, leading to inaccurate results at the onset of fracture.

As an extension, model C was introduced recently (Rots, Belletti and Invernizzi [2]). Here, a ripple of fixed strength range is preset by the user, and the consecutive reduction of both E and f_t is recalculated from the shape and area underneath. Also the number of saw-teeth required then results from this automatically. This generic "ripple model" turns out to be superior, for two reasons. First, the actual position of the local peaks is always close to the softening envelope, within the strength range specified by the user. A undershoot at the beginning, as in model A and B, cannot occur. In fact, the specified strength range can be seen as a local tolerance or convergence criterion, similar to global convergence criteria in Newton-Raphson strategies. Secondly, the ripple model is generic. Any stress-strain diagram can be approximated or "rippled", not only a linear softening diagram, but also a nonlinear exponential softening diagram (model D), or a plastic crushing diagram for concrete (Fig. 2a), or an elastic-plastic stress-strain diagram for reinforcing steel (Fig. 2b). In this way, both quasi-brittle cracks, crushing zones as well as ductile failure modes in reinforced concrete or reinforced masonry structures can be simulated in a generic way.

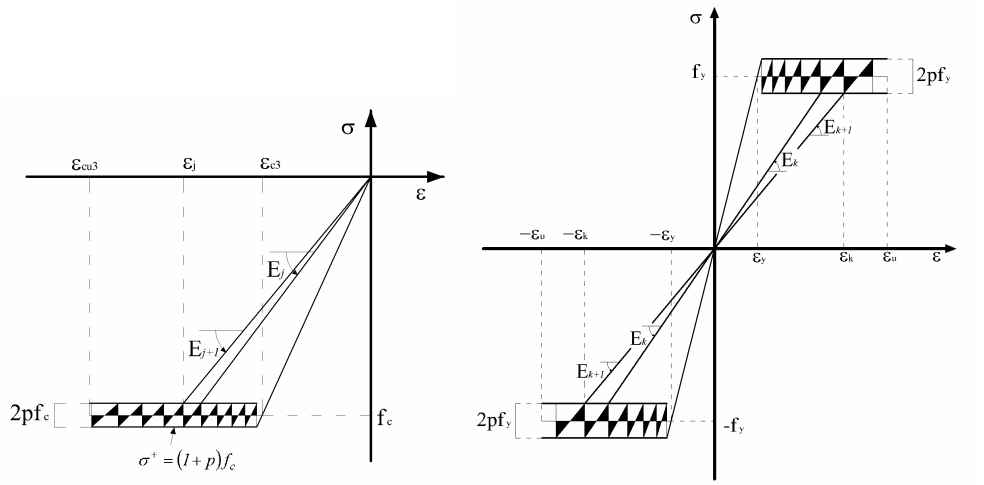

Figure 2: Ripple saw-tooth model for crushing in compression (left) and for steel plasticity (right)

4. Examples

In [1,2] it has been shown that the models always provide a solution: the secant saw-tooth stiffness is always positive, so that ill-conditioning or divergence does not appear in sequentially linear analysis. An advantage is that regular notions of fracture mechanics, like the principal tensile stress criterion, the strength and fracture energy are maintained; this helps in adopting realistic energy consumption and toughness parameters as

observed in experiments. Also, objectivity with respect to mesh refinement was demonstrated. Fig. 4 shows an example for a deep reinforced concrete beam. Here, both the snap-back associated with the brittle sudden occurrence of a major crack emerges in a natural fashion, as well as the final ductile plateau associated with rebar plasticity.

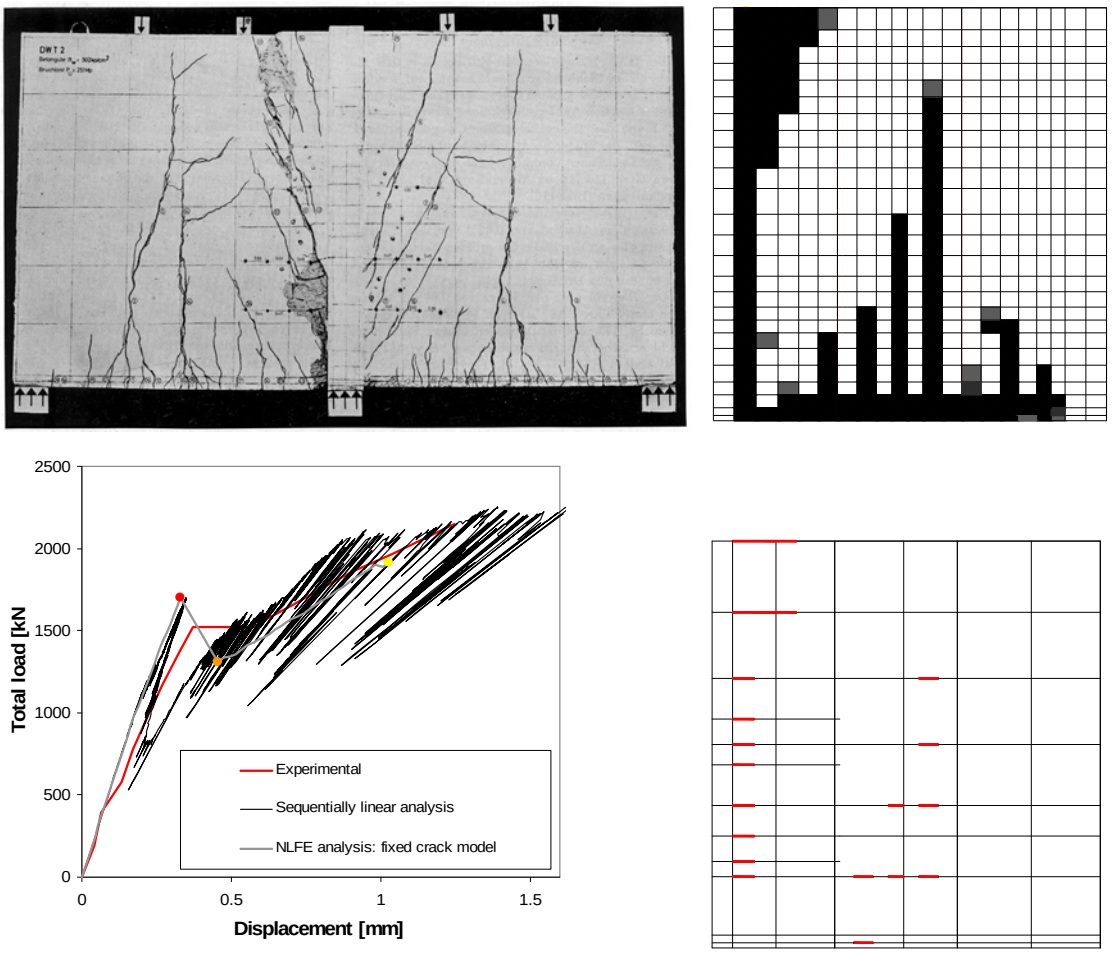

Figure 3: Deep reinforced beam. Experiment (left top), load-displacement response (left bottom), crack pattern as saw-tooth damaged elements (right top), reinforcement saw-tooth plasticity (right bottom) [2].

5. Non-proportional loading

In structural practice, often a non-proportional combination of two loads occurs, e.g. dead load followed by a prescribed settlement, or dead load followed by a horizontal wind load. Hence, it is important to have a scaling procedure that can handle the two loads, an initial load A and a subsequent load B. DeJong et al. [3] recently developed, implemented and evaluated such extension towards non-proportional loading. Cracking is limited to occur during application of load B. The procedure is as follows:

- Apply load A and calculate stresses, σ_A, and then remove load A.
- Apply an increment of load B and calculate stresses, $\Delta\sigma_B$.
- Calculate the load multipliers, $\lambda_{1,2}$, at which the maximum principal stress resulting from the combination of loads A and B ($\Delta\sigma_B + \lambda_{1,2} * \Delta\sigma_B$) equals the current tensile strength, f_{ct} (see Section 3.2).
- Determine the critical integration point and calculate λ_{crit} . Here, alternative selection criteria are necessary. For details, see DeJong et al. [3].
- Apply the critical load combination $\Delta\sigma_B + \lambda_{crit} * \Delta\sigma_B$ to obtain the current stress-strain state.

- Remove all loads and update the stiffness and strength properties of the critical integration point according to the saw-tooth constitutive model (see Section 2.2).
- Repeat this cycle of steps continuously, updating the properties of a single integration point after each cycle.

Fig. 4 shows an example of a beam subjected to pre-stress as well as four-point bending. Both compressive and tensile pre-stress have been analyzed. The results closely resemble the actual nonlinear reference result, demonstrating the effectiveness of the non-proportional scheme. Finally, the method was applied to a masonry façade subjected to dead load and line loads, followed by a subsequent settlement trough. The example was published before, both incremental-iteratively with unstable behavior, as well as sequentially by ignoring the dead load [1]. Now, the snap-back behaviour for the non-proportional case can be handled, see [3].

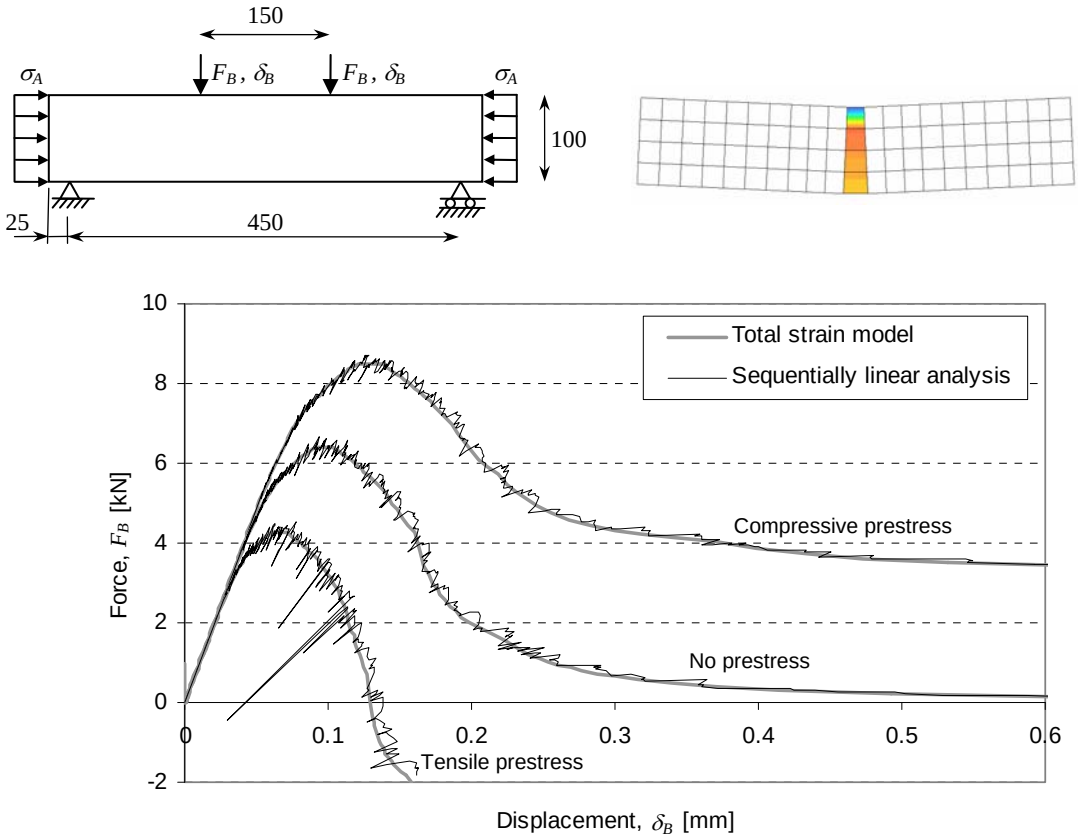

Figure 4: Non-proportional analysis of beam with pre-stress and four-point bending.

References

[1] Rots JG, Invernizzi S. Regularized sequentially linear saw-tooth softening model. *Int. Journal for Numerical and Analytical methods in Geomechanics* 2004; **28**: 821-856.

[2] Rots JG, Belletti B. and Invernizzi S. Robust modeling of RC structures with an "event-by-event" strategy. *Engineering Fracture Mechanics* 2008; **75**: 590-614.

[3] DeJong MJ, Hendriks MAN and Rots JG. A sequentially linear approach to modeling fracture under non-proportional loading. Submitted for publication, April 2008.

Proceedings of the 6th International Conference on
Computation of Shell and Spatial Structures
IASS-IACM 2008: "Spanning Nano to Mega"
28-31 May 2008, Cornell University, Ithaca, NY, USA
John F. ABEL and J. Robert COOKE (eds.)

The multi-scale approach of masonry, paradigm of clay brick.

Konrad J.KRAKOWIAK*, Paulo B. LOURENÇO, Franz-J. ULM

*PhD Student
University of Minho, School of Engineering, Civil Engineering Department
konrad@civil.uminho.pt

Abstract

Recent progress in nanoscience and engineering allows advanced characterization of materials. This type of characterization includes investigations revealing the scale dependent microstructure and mechanical as well physical properties of each component incorporated in the heterogeneous material. Its applicability and efficiency is confirmed in the field of cement based materials where the paradigm of these materials is solved, and universal buildings blocks and the multi-scale nature are well described. As a consequence, material researchers and engineers have knowledge about the impact of basic constituents and microstructure on macro behaviour of cement based materials. In the masonry field, a quite diverse situation is found. Although clay brick is among the oldest building materials, the main building blocks are still unknown. This knowledge gap is apparent in structural masonry, since the present homogenization and upscaling techniques consider only mortar joints, brick units and interface as a basic units. Here, the mechanical properties and elementary arrangement of these three components in the representative volume element (RVE) are assumed to govern the behaviour of masonry as a composite. But, it is understood that mortar may be broken down to lower scales, and its macro mechanical properties considered in the already developed approaches are governed by the lover scale components and its microstructure. Similarly, as it is shown by the authors in this contribution the brick unit may be broken down to lower scales, in which the basic material components and theirs properties are inherent. Therefore, the macro behaviour of composite masonry wall and its durability is considered to be ruled by the phenomena from the much lower scales present in the mortar, clay brick and the interface of these two.

1. Introduction

Masonry walls, pillars etc. are composite structures which consist of mortar joints and units of clay brick, concrete blocks, calcium-silicate blocks, etc.. Most of the masonry structural elements have one common characteristic: the units are stacked in a periodic way. Due to this special future, the homogenization technique of periodic media is very popular among researchers (Lourenço [6]) as a tool for structural analysis of large scale structures, rather than a detailed micro-modeling approach. Macro and micro-modeling approaches departs from the scale of $>10^{-2}m$, where the materials properties of mortar, brick and interface represent the macro properties of these components obtained in laboratory tests. However, it is known that the mechanical performance of materials depends on their morphology and phase constitution, in case of a composite. Therefore, it is correct to assume that the structural behaviour of masonry on engineering scale is ruled by the phenomena existing on scales much lower than $>10^{-2}m$, which are related with microstructure of mortar, clay brick and eventually theirs interface.

Recent studies in material science revealed the existence of microstructural features of mortar on lower scales. As a consequence, its macro-properties and macro-behaviour is governed by lower scales phenomena. Mortar, according to this multi-level representation is a material with four levels of microstructure, which obeys the principle of separation of scales (Ulm [7], Constantinides [3]). In this hierarchy Level "0" is associated with nanoscale and single colloidal particle of C-S-H solid. Changing the scale order leads to Level "I", of hundreds nanometers, where the single particles tend to agglomerate to form C-S-H gel matrix with gel porosity. Level "II" represents the structure of cement paste, which is formed from C-S-H matrix, large Portlandite crystals,

unhydrated cement clinker and macroporosity. In the last level (Level "III"), the sand particles and interfacial transition zone (ITZ) are incorporated. This think model of mortar morphology, together with results of experimental characterization of mechanical properties of existing phases and advanced mathematical methods of micro-poromechanics allows bridging the existing scales and relating properly the material macro-properties with its microstructure and composition.

The research carried out here is directed towards understanding the microstructural paradigm of clay brick, combining it with a microstructural model of mortar, and bridging it with existing approaches in structural masonry, see Figure 1. This endeavour includes the definition of material scales for the clay brick and the classification of the morphological futures present at each level of observation. The chosen strategy closes the existing gap in the masonry science regarding multi-scale modeling. Moreover, it establishes the solid link between the lowest material levels and the scale of engineering applications for masonry. By doing so, the authors believe see new directions for the development of optimal and sustainable masonry constructions, where the influence of changes of the main building blocks on structural performance and durability of masonry may be easily captured.

Some attempts to explore the clay brick material characteristics were done in the past and recent years. However, they are focused mainly on separated sub-domains of this complex problem like: phase transformation during the firing process (Grim [5], Brindley [1]), influence of raw materials and brick processing on global physical and mechanical properties of brick (Cultrone [4], Freyburg [2]), or attempt the general characterization of construction materials.

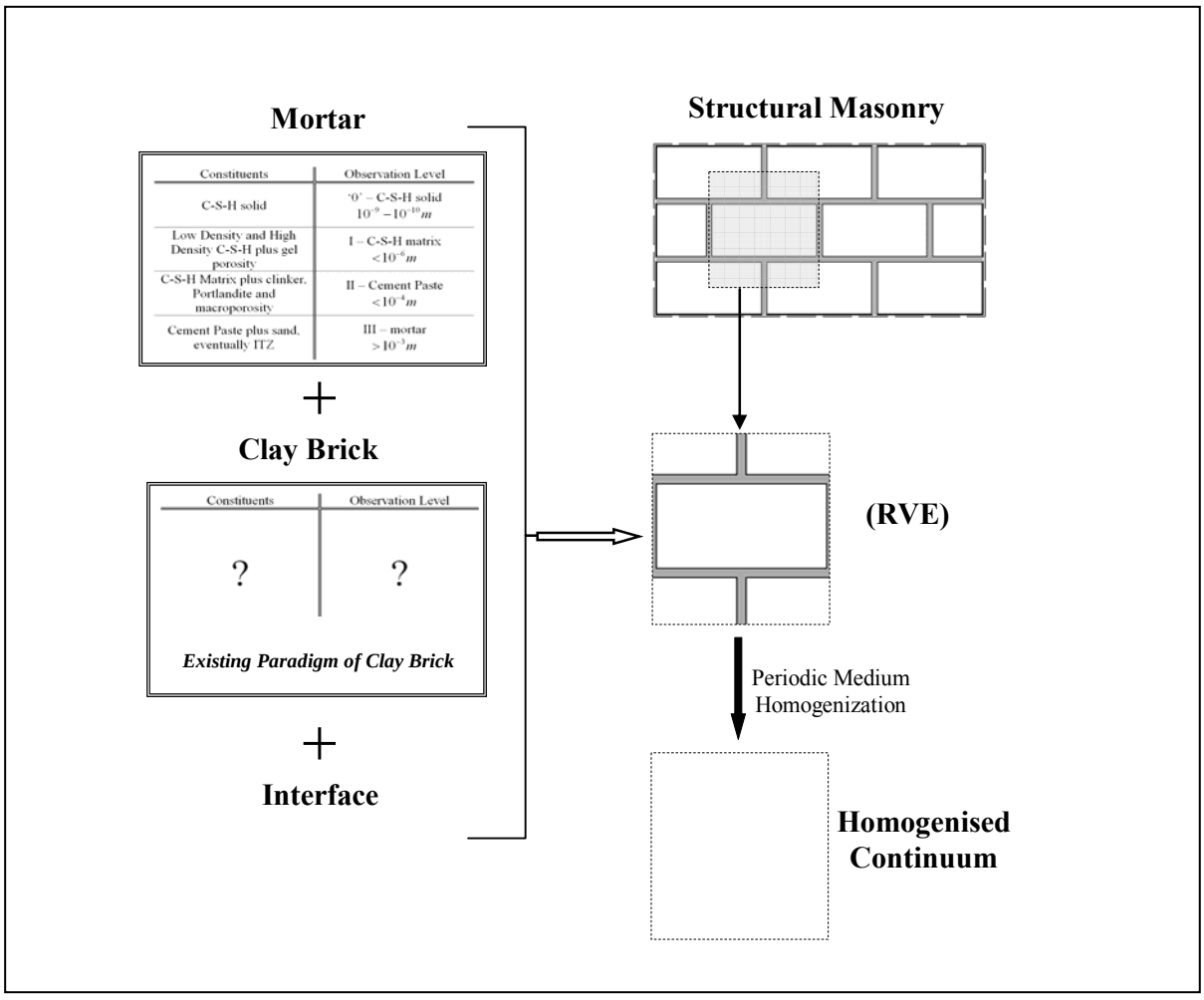

Figure 1: Assumed strategy to combine material scales within masonry

2. Experimental part

Characterization of the morphology of clay brick is carried on the samples obtained from the production lines of three Portuguese plants. The collected samples represent different classes of masonry bricks: facing brick, standard quality brick and low quality brick representing ancient masonry constructions. The characterization of bricks includes: classification of existing phases by X-Ray Diffraction, optical microscopy etc.; porous network description and microstructural arrangement are evaluated with use of SEM/AFM/TEM Microscopy, Mercury Intrusion Porosimetry, and traditional gravimetric methods; identification of mechanical properties of constituents at smallest scales by massive grid nanoindentation; macro strength and stiffness coefficients obtained by standard laboratory means and procedures.

The results obtained during the first period of research clearly indicate the existence of the 'glassy' matrix, aggregates of different size and porous domain Figure 2. The constituents are common for all types of samples. However, investigation of firing processes and raw materials composition indicates varying concentration of each phase with respect to the origin of sample, its firing history and raw material composition. The brick fired briefly at 1030ºC and cooled relatively fast has lower 'glass' matrix concentration. On the other hand, samples prepared in the traditional fashion with long maturing in 980ºC and relatively slow cooling rate are characterized by higher concentrations of 'glassy' matrix.

The investigated 'glassy' matrix is an amorphous, brittle material. Its volume fraction, together with the fraction of embedded crystal aggregates, strongly influences the mechanical properties of fired clay. Higher concentration of amorphous phase decreases the body strength and increases material brittleness. These observations are consistent with experimental results carried on macro scale.

The aggregates exist in three different forms: crystals embedded in the glass (order of nanometers), silt ($10^{-6} - 10^{-3} m$) and sand grains ($> 10^{-3} m$). The first type is the result of the viscous phase crystallization during cooling of brick in the firing cycle. Its concentration and concentration of glass phase are interrelated. Their volume fraction depends on the volume of the finest fraction grains in the raw materials, see Figure 3, as well as the maturing and cooling rate of the green body. The two other types of aggregates are the grains of silt and sand. The first fraction of raw material is partially affected by high temperature, and large percentage of it remains in the form of embedded grains. The sand fraction remains unaffected in the firing process. They are composed of mineral quartz. With respect to its hardness they form the back bone of fired brick and reinforce the material in similar way like in gravel aggregate in concrete.

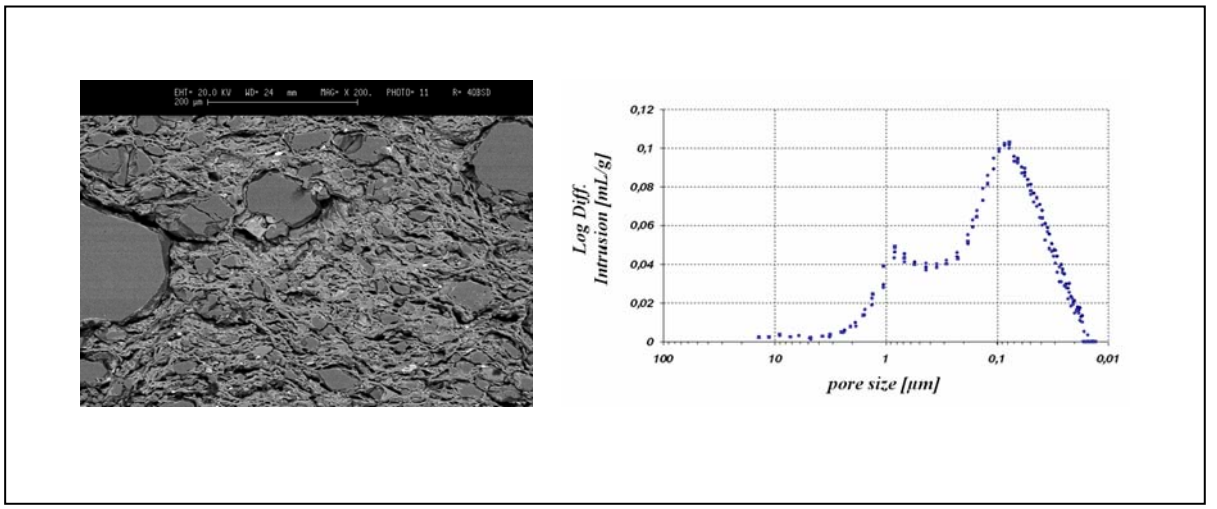

Figure 2: SEM image of clay brick microstructure; strings of 'glassy' matrix, fine and coarse aggregates and porous domain (left). Pore size distribution in engineering brick dominated by nano and micro pores (right)

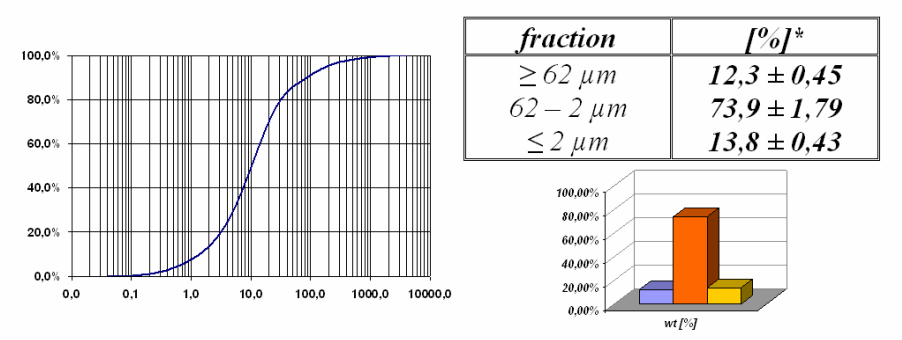

Figure 3: Grain size distribution of raw material: fine fraction (< 2 μm, yellow) is incorporated completely in the 'glassy' matrix; a part of the silt (62-2 μm, orange) is partially incorporated in matrix; sand (> 62 μm, blue) remains untouched in the form of large aggregates

The porous domain is in all cases oriented in the direction of the green body extrusion. It is the result of alignment of clay particles with respect to the flow lines of extruded mass. This feature is well visible in the SEM images of microstructure, see Figure 2. In this image the pores, represented by black colour, are obviously elongated along horizontal direction. Another important feature noted during this research is the brick lamination, which is the result of shaping technology (soft extrusion).

Acknowledgement

The authors gratefully acknowledge the Portuguese Foundation of Science (FCT) for providing the PhD grant for doctoral student Konrad. J. Krakowiak. The authors also thank João Paulo de Castro Gomes and Centre of Materials and Building Technologies, UBI, Portugal for support in the MIP measurements.

References

[1] Brindley GW, Udagawa S. High temperature reactions of clay mineral mixtures and their ceramic properties, In *Journal of the American Ceramic Society*, 1960; 43; 2

[2] Freyburg S. Schwarz A. Influence of the clay type on the pore structure of structural ceramics, In *Journal of the European Ceramic Society*, 2007; 27; 1727-1733

[3] Constantinides G. Invariant Mechanical Properties of Calcium-Silicate Hydrates (C-S-H) in Cement-Based Materials: Instrumented Nanoindentation and Microporomechanical Modeling, *PhD Thesis*, 2006, Massachusetts Institute of Technology

[4] Cultrone G, Sebastián E, Elert K, de la Torre MJ, Cazalla O, Rodriguez-Navarro C. Influence of mineralogy and firing temperature on the porosity of bricks, In *Journal of the European Ceramic Society*, 2004; 24; 547-564

[5] Grim RE, Johns WD. Reactions accompanying the firing of brick, In *Journal of the American Ceramic Society*, 1951; 34;3

[6] Lourenço PB. Analysis of masonry structures: review of and recent trends in homogenization techniques, In *Canadian Journal of Civil Engineering*, 2007; 34; 1443-1457

[7] Ulm F-J. Chemomechanics of concrete at finer scales, In *Materials and Structures*, 2003; 36:426-438.

Proceedings of the 6th International Conference on
Computation of Shell and Spatial Structures
IASS-IACM 2008: "Spanning Nano to Mega"
28-31 May 2008, Cornell University, Ithaca, NY, USA
John F. ABEL and J. Robert COOKE (eds.)

Simplified modeling strategies for non linear dynamic calculations of RC structural walls including soil-structure interaction

P. KOTRONIS*, J. MAZARS, S. GRANGE, C. GIRY

* Laboratoire Sols Solides Structures-Risques (3S-R), Grenoble Universités, CNRS
Domaine Universitaire BP 53, 38041 Grenoble cedex 9, France
Panagiotis.Kotronis@inpg.fr

Abstract

This paper presents "blind" numerical calculations using multifiber beam elements, damage mechanics and plasticity constitutive laws. The calculations were performed in laboratory Sols Solides Structures-Risques (3S-R) in order to participate to two international benchmarks (NEES and SMART 2008) dealing with the non linear dynamic behavior of reinforced concrete structural walls tested on shaking tables. A numerical tool for simulating Soil-Structure Interaction (SSI) is also presented. The new element is based on the "macro element" concept and it is used to perform parametrical studies on the NEES structure considering different types of soils.

1. 7-story building (Benchmark NEES): Numerical modeling and influence of SSI

The University of California at San Diego (UCSD), the Portland Cement Association (PCA) of Skokie, IL., and the NEES Consortium Inc (NEESinc) have performed a seismic research project around an uniaxial shaking table test on an embedded mock-up representing a full-scale vertical slice of a seven-story reinforced concrete wall building. The specimen is composed of two perpendicular walls linked with slotted connections and it is considered embedded on the shaking table (NEES [8]).

Multifiber Timoshenko beam elements are used to reproduce numerically the experimental behavior of the structure (Kotronis and Mazars [5]) (Figure 1). The constitutive models used are: La Borderie [6] damage model for concrete and Menegoto-Pinto [7] model for steel. Concentrated masses are considered at each floor taking into account the mass of the corresponding slab and the upper and lower part of the wall. Calculations have been performed with FEDEASLab developed at UC Berkeley.

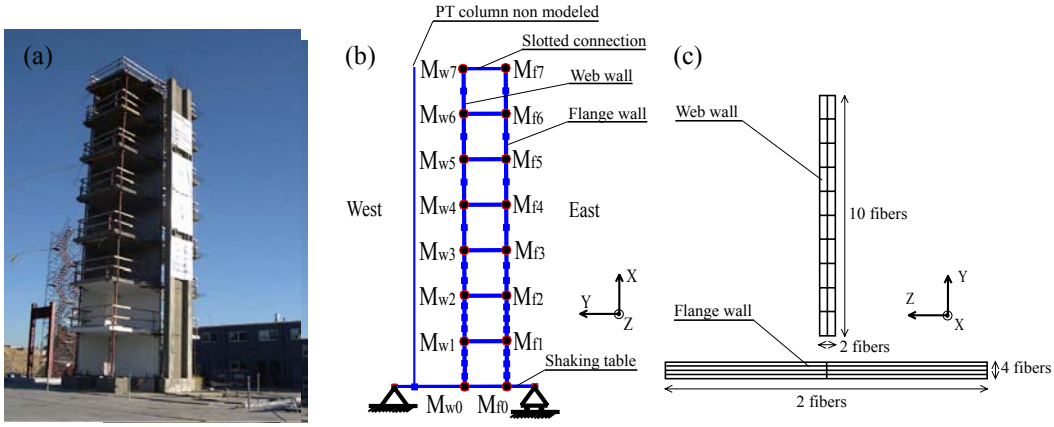

Figure 1: Photo of the NEES building and multifiber mesh

It is shown that the modeling strategy describes accurately the global behavior of the structure (figure 2) and qualitatively the distribution of damage.

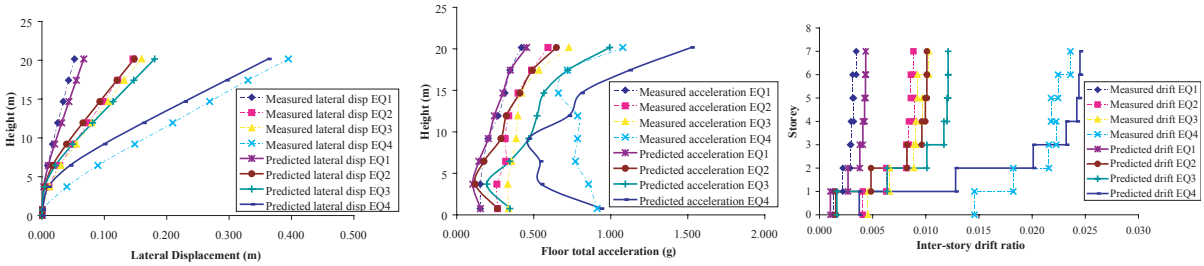

Figure 2: NEES building - Maximum lateral displacements, accelerations and inter-story drift ratio at different levels of the structure for 4 sequences, comparisons between experimental (dotted lines) and "blind" prediction numerical results (continuous lines).

Moreover, this simplified approach helps reducing computational costs. It appears now possible to use this kind of modelling strategy to investigate numerically the behaviour of a wider variety of configurations that is practically impossible to study experimentally. Following this remark we investigate hereafter the influence of SSI on the behaviour of the NEES structure for 5 different types of soils going from very low characteristics soil (soil 1) to very high characteristics soil (soil 5).

The NEES structure is considered now posed on a new SSI macro element taking into account plasticity of the soil and uplift of the foundation (Grange [1], Grange *et al.* [2]). In other words, the structure is supposed to have a rigid shallow and rectangular foundation lying on the soil (dimensions 4.5m x 2.8m).

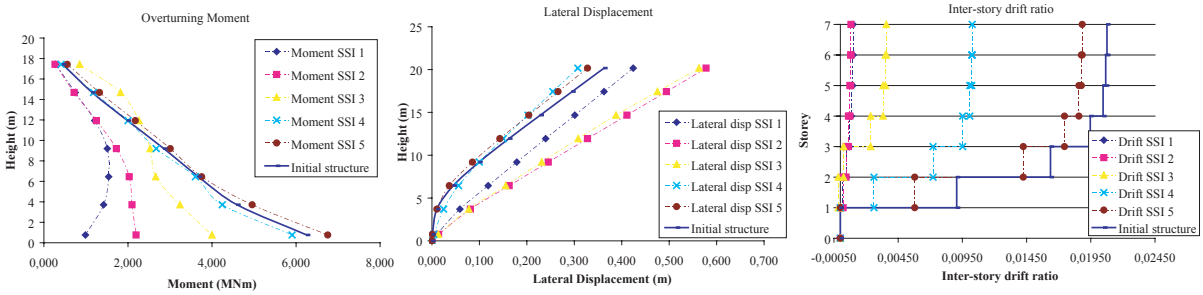

Figure 3: NEES building - Maximum overturning moments, lateral displacements, and inter-story drift ratio at different levels of the structure for the sequence EQ4, for the 5 different soils (dotted lines) and the structure considered embedded on the shaking table (continuous lines).

Results show that SSI decreases the forces at the base of the building (figure 3) and changes the influence of the higher modes. Using the Karhunen-Loéve method (Gutiérrez and Zaldivar [4]) one can perform a modal decomposition and show that mode 2 is preponderant for soils 1 and 2 but mode 3 influences mainly the behavior of the structure lying on soil 3. This change in the behavior can lead to a concentration of damage at the upper levels of the building, develop smaller lateral displacements but more important residual forces.

3. Benchmark SMART 2008: Numerical modeling

In the last years, a large number of dynamic experimental tests have been performed on structural elements or entire structures. However, the investigation of 3D-phenomena (like torsion) is rare. This is the context of the "SMART 2008" benchmark (Seismic design and best-estimate Methods Assessment for Reinforced concrete buildings subjected to Torsion and non-linear effects [9]) organized by the Comissariat à l'Energie Atomique (CEA Saclay, France). The purpose is to study the behavior of a non symmetrical building (Figure 4) at a scale ¼ under seismic loading applied thanks to the shaking table of CEA. The strategy adopted in 3S-R to model the structure is the use of Timoshenko multifiber beams (Figure 4) associated with constitutive laws based on

damage mechanics for concrete and plasticity for steel. This choice allows reducing considerably the time of calculation without loosing access to information needed in order to analyze the behavior of the structure (displacements, base forces, stresses, strains, damage…). Calculations have been performed with the Finite Element Code Cast3m (version 2007) developed by CEA.

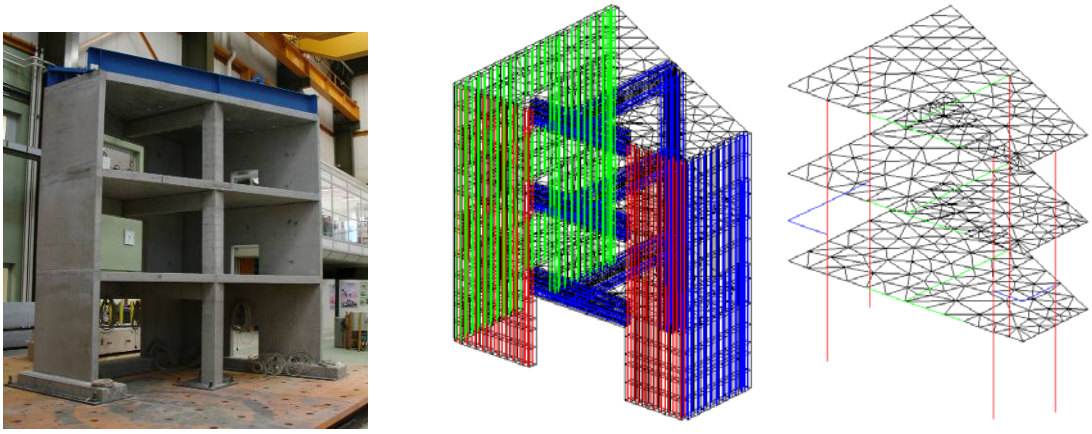

Figure 4: Photo of the SMART 2008 building and multifiber mesh

The different walls, the columns and the beams are represented by Timoshenko multifiber beams (Guedes *et al.* [3]) with La Borderie [6] damage model for concrete and Menegoto-Pinto [7] model for steel. The floors are represented by shell elements having a linear behavior. The links between the walls are reproduced through a rigid element between the first and the second floor.

1er mode F = 9,96 Hz	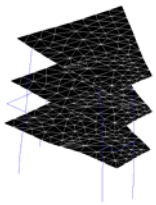	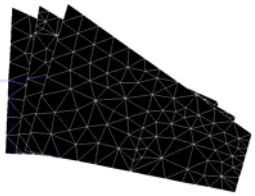
2nd mode F = 16,01 Hz	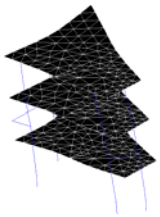	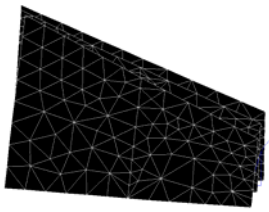
3ème mode F = 32,21 Hz	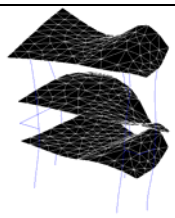	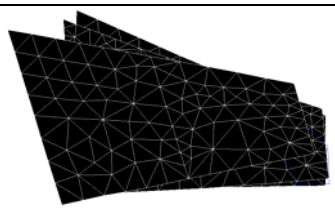

Figure 5: The first three modes of the SMART 2008 structure

The different modes of vibration of the structure (Figure 5) present the same tendency as the ones that have been obtained with more complex modeling strategies (i.e. multilayer shell elements, 3D elements). The evolution of the displacement at the top of the structure (Figure 6) under a provided earthquake sequence is presented in (Figure 7, “blind” results).

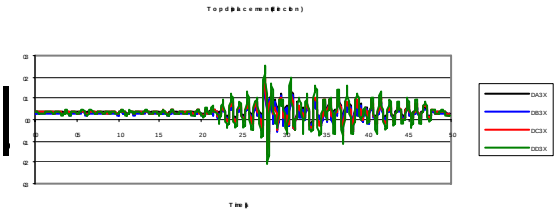

x-direction

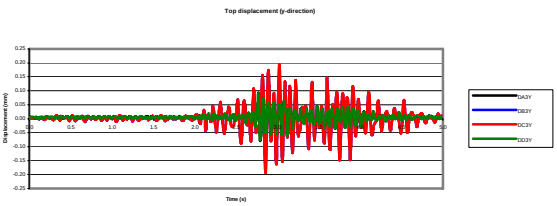

y-direction

Figure 6: SMART 2008 structure - Top displacement

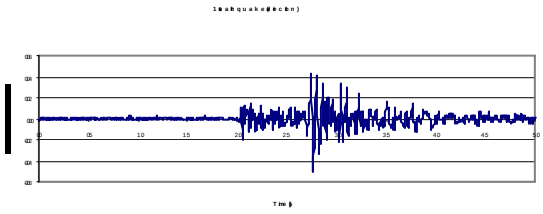

x-direction

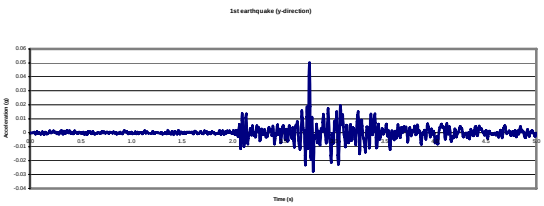

y-direction

Figure 7: Earthquake loading (0.05g)

The entire calculation for the 13 loading sequences provided by the organizers of the benchmark needs only 2 or 3 days with a recent computer whereas it can take several weeks for a multi-layer shell modeling and even more for 3D-element. Although 3D behavior like torsion and interaction between elements of the structure are still points that can be improved, Timoshenko multifiber beams are definitely an important tool for the practical engineer for the next years. The experimental campaign on the structure is scheduled by the beginning of July 2008.

References

[1] Grange S. Risque sismique: stratégie de modélisation pour simuler la réponse des structures en béton et leurs interactions avec le sol., Thèse d'état *INPG*, (en préparation).

[2] Grange S., Kotronis P. and Mazars J. « A 3D macro-element for soil-structure interaction ». *International Journal for Numerical and Analytical Methods in Geomechanics*, (early view), 2007.

[3] Guedes J., Pégon P and Pinto A. « A fibre Timoshenko beam element in CASTEM 2000 ». Special publication Nr. I.94.31, JRC, I-21020 Ispra, Italy, 1994.

[4] Gutiérrez E and Zaldivar JM. The application of Karhunen-Loéve, or principal component analysis method, to study the non-linear seismic response of structures. *Earthquake Engng Struct. Dyn.* 2000; **29**:1261–1286.

[5] Kotronis P. and Mazars J. « Simplified modelling strategies to simulate the dynamic behaviour of R/C walls ». *Journal of Earthquake Engineering*, **9**-2, pp.285-306, 2005.

[6] La Borderie CL. Phénomènes unilatéraux dans un matériau endommageable : modélisation et application à l'analyse des structures en béton, Thèse d'Etat, Université Paris 6, 1991.

[7] Menegoto M. and Pinto P. Method of analysis of cyclically loaded reinforced concrete plane frames including changes in geometry and non-elastic behaviour of elements under combined normal force and bending, IABSE Symposium on resistance and ultimate deformability of structures acted on by well-defined repeated loads, final report 328p, Lisbon, 1973.

[8] NEES at UCSD « Seven-Story Building-Slice Earthquake Blind Prediction Contest » http://nees.ucsd.edu/7Story.html , NEES7story, 2006

[9] Lermitte S. and Chaudat T. SEMT/EMSI/PT/07-003/C. Presentation of the blind prediction contest– SMART 2008 project.

Proceedings of the 6th International Conference on
Computation of Shell and Spatial Structures
IASS-IACM 2008: "Spanning Nano to Mega"
28-31 May 2008, Cornell University, Ithaca, NY, USA
John F. ABEL and J. Robert COOKE (eds.)

Modeling mixed-mode crack propagation in reinforced concrete

Rena C. YU*, Gonzalo RUIZ, Jacinto R. CARMONA

*University of Castilla-La Mancha
Avda. Camilo José Cela,
13071 Ciudad Real, Spain
Email: rena@uclm.es

Abstract

We propose a methodology to model mixed mode crack propagation in reinforced concrete beams subjected to static loading. The discrete cohesive approach, accompanied by an insertion algorithm, is adopted and a modified dynamic relaxation method is chosen as an alternative solver. The concrete matrix and steel re-bars are modelled explicitly; the connection in between is represented by means of interface elements. The methodology is validated against three-point bending beams with notches shifted from the middle span.

1. Introduction

In this paper we investigate the evolution of 3D complex fracture processes in reinforced concrete specimens subjected to static loading. We endeavour to model explicitly the mixed-mode fracture in concrete bulk and debonding of the re-bar. We simulate the concrete matrix, the steel re-bars and the interface between the two materials explicitly. The cracks in the concrete matrix are described by using cohesive theories of fracture combined with the direct simulation of fracture and fragmentation. In reinforced concrete, the crack advancing through the concrete matrix is hindered by the presence of reinforcing bars. The development of the cracking process from then on implies the deterioration of the interface, which is modelled by inserting interface elements endowed with an effective adherent law along the steel-concrete contact. As the external loads increase the cracks in the matrix are finally able to propagate through the steel bar. Thus, the sewing effect of the steel bars is modelled explicitly. The difficulty of looking for a stable solution is avoided by means of the dynamic relaxation method, which always succeeds in finding a solution if such a solution exists. The slow convergence of the method is compensated for by means of a modified technique, see Yu and Ruiz [1, 2]. The feasibility of the proposed methodology is validated against fracture tests on reinforced beams in flexure (Carmona, Ruiz and Viso [4]).

2. Finite element methodology

2.1 Cohesive theory of fracture

For completeness and subsequent reference, we outline the main features of the cohesive law and the interface constitutive law used in our calculations. A more detailed account of the theory and its finite-element implementation can be found elsewhere, see Ortiz and Pandolfi [3] for example. A variety of mixed-mode cohesive laws accounting for tension-shear coupling are established by the introduction of an effective opening displacement w,

$$w = \sqrt{\beta^2 w_s^2 + w_n^2} \tag{1}$$

which assigns different weights to the normal and sliding opening displacements. Supposing that the cohesive free-energy density depends on the opening displacements only through the effective opening displacement w, a reduced cohesive law, which relates w to an effective cohesive traction.

$$t = \sqrt{\beta^{-2} t_s^2 + t_n^2} \tag{2}$$

where t_s and t_n are the shear and the normal tractions respectively, can be obtained. The weighting coefficient β is considered a material parameter that measures the relationship between the shear and tensile resistance of the material.

2.2 A modified dynamic relaxation method as an alternative solver

The crack propagation was led by a fragmentation algorithm that was able to modify the topology of the mesh at each loading step. This inevitably induces high geometric roughness upon the existing material non-linearity, hence a challenge for most implicit solvers when searching for static solutions. To avoid this problem, we consider the explicit dynamic relaxation (DR) method as a feasible alternative solver. One of the common difficulties with the DR method is its slow convergence rate when non-monotonic spectral response is involved. We adopt a modified technique illustrated in Yu and Ruiz [1] in order to sidestep this difficulty. Instead of critically damping the system of equations from the beginning, as suggested by all the standard DR procedures, the motion is kept as *strong* as possible. Through *under-damping* the system, the local movement provoked at the loading area or the crack tip can spread to the rest of the system; in this way the convergence rate is significantly improved.

2.3 Experimental setup

In order to validate the numerical methodology, we choose an experimental program reported by Carmona, Del Viso and Ruiz [4]. The program was designed to study mixed mode crack propagation in reinforced concrete. In addition, an exhaustive material characterization to allow a complete interpretation of the test results was provided. The tests were carried out on beams off-notched from the mid-span. A single, mixed-mode, macro crack carried on to the entire loading process, see Figure 1. The load P, and the displacement under the load point δ, were continually monitored and recorded. A resistive extensometer centered on the tensioned face of the beam at the mouth of the notch was used to measure the crack opening displacement *CMOD*. The mechanical properties of concrete and its characteristic length are shown in Table 1; the parameters for steel and the bond-slip strength of the steel-concrete interface are given in Table 2.

f_c (MPa)	f_{ts} (MPa)	E_c (GPa)	G_F (N/m)	l_{ch} (mm)
36.3	3.8	28.3	43.4	86.8

Table 1 Concrete mechanical properties.

E_s (GPa)	f_{ts} (MPa)	f_u(MPa)	ε_u (N/m)	τ_c (MPa)
174	563	632	4.6	6-8

Table 2 Steel mechanical properties and the interface bond strength.

3. Numerical results

We compare the numerical simulations against the experimental data for a three point bend tests on a 150mmx75mmx600 mm beam. The beam is reinforced with 2 longitudinal ribbed bars of 2.5 mm of diameter, this gives a reinforcement ratio of 0.13%. The comparison of P-δ, P-CMOD and crack patterns are shown in Figures 1a, b and c respectively. The numerical model captures the peak load, the crack trajectory, the debonding and micro cracking around the bars at the notch position. The overall performance is remarkable,

taking into consideration that all the material parameters fed to the numerical model were directly measured in the experiments.

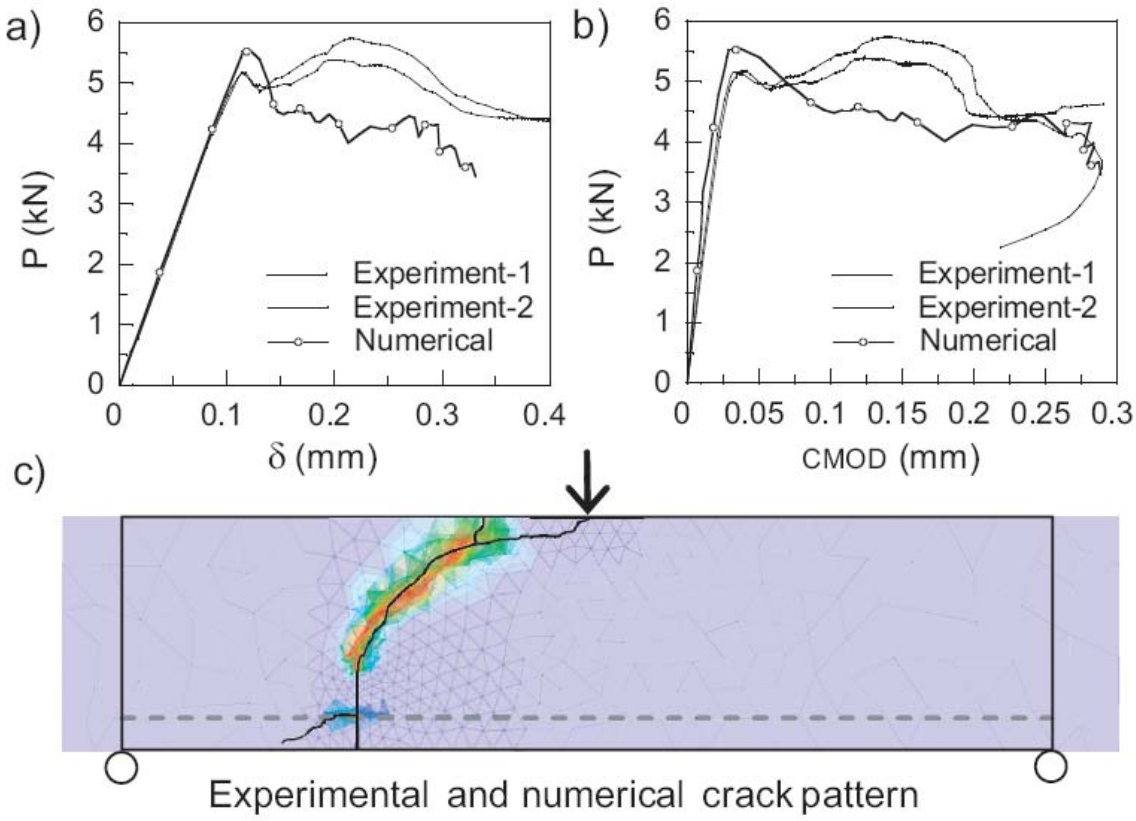

Figure 1 Numerical and experimental comparison (a) P-δ curve (b) P-*CMOD* curve (c) crack pattern.

Acknowledgement

The financial support from the Spanish Ministry of Education and Science through grant MAT2006-09105 is acknowledged.

References

[1] Yu RC and Ruiz G. Static multi-crack modelling in concrete solved by a modified DR method. *Computers and Concrete* 2004; **1(4)**:371-388.

[2] Yu RC and Ruiz G. Explicit finite element modelling of static crack propagation in reinforced concrete. *International Journal of Fracture* 2006; **33**:1413-1449.

[3] Ortiz M and Pandolfi A. Finite-deformation irreversible cohesive elements for three-dimensional crack propagation analysis. *International Journal for Numerical Methods in Engineering* 1999; **33**:1267-1282.

[4] Carmona JR, Del Viso JR and Ruiz G. Mixed-mode crack propagation through reinforced concrete. *Engineering Fracture Mechanics* 2007;**74:**2788-2809.

Proceedings of the 6th International Conference on
Computation of Shell and Spatial Structures
IASS-IACM 2008: "Spanning Nano to Mega"
28-31 May 2008, Cornell University, Ithaca, NY, USA
John F. ABEL and J. Robert COOKE (eds.)

Limit-analysis based identification of fracture and degradation mechanisms in two-phase composite materials

Josef Füssl*, Roman Lackner

*Institute for Mechanics of Materials and Structures, Vienna University of Technology
Karlsplatz 13/202, 1040 Vienna, Austria
Josef.Fuessl@tuwien.ac.at

Abstract

Upscaling of strength properties of two-phase composite materials (matrix and particles/air-voids) is performed using numerical limit analysis formulations, accounting for the discontinuous nature of material failure. Moreover, the effect of the interface-transition zone between matrix and particles, which may be weakened by chemical and thermal processes during construction and operation, is considered. Limit analysis gives access to lower and upper bounds of the material strength. Moreover, microstructure-based effective failure surfaces can be derived for different states of degradation of the material system.

1. Limit analysis formulations

Originally, the objective of limit analysis was determination of the load-bearing capacity of structures exhibiting elastoplastic material response. At collapse, structures have exhausted their capacity to store any additional external work as recoverable energy. Thus, for a given macroscopic strain-rate field and a prescribed macroscopic stress field defining the loading situation, limit analysis concentrates on the critical work rate at failure of structures or, as in our case, of composite materials.

For the *numerical upper-bound (UB) formulation*, 6-node triangular linear-strain elements for the 2D situation and 10-node tetrahedral linear-strain elements for the 3D situation with plane surfaces are used. For both element types, quadratic shape functions for the interpolation of the unknown velocity field are used (Makrodimopoulos and Martin [3]). If the vertices of the linear-strain elements are taken as the flow-rule points, the obtained solutions are strict upper bounds on the exact collapse load. For the stress field, a linear stress distribution is assumed within each element. To enforce the admissibility of the velocity-field solution within the UB formulation, the following conditions are imposed: (i) The strain rate must follow an associative flow rule and (ii) the velocity field has to fulfill either linear velocity boundary conditions $\mathbf{u}(\mathbf{x}) = \mathbf{E}\mathbf{x}$ or periodic boundary conditions $\mathbf{u}(\mathbf{x}) = \mathbf{E}\mathbf{x} + \mathbf{u}^{\mathrm{p}}(\mathbf{x})$. In accordance with commonly employed analytical schemes for upscaling of mechanical properties subjecting the considered representative volume element (RVE) to linear velocity boundary conditions, the same boundary conditions may be employed when using the RVE approach for upscaling of strength properties. Periodic boundary conditions, however, allow the evolution of distinct failure zones at the boundary of the RVE and, therefore, show improved performance in capturing the localized nature of material failure. These periodic boundary conditions are essential in case of the unit-cell (UC) approach, ensuring continuity of the velocity field between adjacent unit cells. $\mathbf{E}$ is a predefined symmetric macroscopic strain-rate tensor and $\mathbf{u}(\mathbf{x})$ denotes the velocity vector at point $\mathbf{x}$ of the boundary of the RVE/UC. Under these conditions, the internal rate of work needs to be minimized.

For the *numerical lower-bound (LB) formulation*, the same finite elements as used in the UB formulation are employed. However, in the LB formulation, the nodal unknowns are the stress tensor. Jumps of the tangential stress components along element edges in 2D and at element surfaces in 3D are admitted (Lyamin and Sloan [2], Makrodimopoulos and Martin [4]). To enforce equilibrium and admissibility of the stress-field solution, the

following conditions are imposed: (i) Within each element, equilibrium is enforced by $\mathrm{div}\left[\boldsymbol{\sigma}(\mathbf{x})\right]=\mathbf{0}$, (ii) at discontinuities, continuity of normal- and shear-stress components is enforced, (iii) the stress field has to fulfill the boundary conditions $\boldsymbol{\sigma}(\mathbf{x})\cdot\mathbf{n}(\mathbf{x})=\alpha\mathbf{t}$ at the boundary A_t where surface tractions $\mathbf{t}$ are prescribed ($\mathbf{n}(\mathbf{x})$ denotes the outward normal unity vector on A_t), and (iv) the stress field associated with plastic collapse has to satisfy $f(\mathbf{x};\boldsymbol{\sigma}(\mathbf{x}))\le 0$, where f denotes the yield function. Under these conditions, the external rate of work is maximized.

The arising optimization problem from the UB and LB formulation is nonlinear, with the nonlinearity introduced by the underlying yield functions only. In case of cone-shaped yield criteria, second-order-cone-programming (SOCP) can be successfully used for finding the optimum (Makrodimopoulos and Martin [3]).

2. Application to matrix-particle materials

The application of limit analysis in the context of upscaling of strength properties of matrix-inclusion morphologies is presented. For this purpose, different material systems, consisting of two or three material phases, are discretized and subjected to different loading states. Different strength properties are assigned to the constituents, i.e., the matrix, the inclusions, and the interfaces. By means of limit analysis, lower- and upper bounds for the material strength are computed for different loading situations (see also Füssl *et al.* [1]).

2.1 2D two-phase materials

Figure 2 shows the plastic zones at failure of a porous material for two different (Σ_1,Σ_2)-pairs and for the RVE and UC approach, respectively. The air-void content f_a is 30% and the matrix obeys the Mohr-Coulomb failure criterion (plane-strain situation) with the cohesion $c=10$ Pa and the friction angle $\varphi=10^\circ$. Both, the RVE approach with linear velocity boundary conditions and the UC approach with periodic boundary conditions give identical failure modes. By varying the loading situation on the considered RVE/UC representing the material microstructure, failure surfaces are obtained for two different principal directions of loading with respect to the material microstructure (see Figure 1). Figure 3(a) shows further failure modes corresponding to different loading situations, defined by the macroscopic strain-rate tensor $\mathbf{E}$. Figures 3(b) show the failure modes of a matrix-particle material with 65% degraded interface loaded by four different macroscopic strain rates.

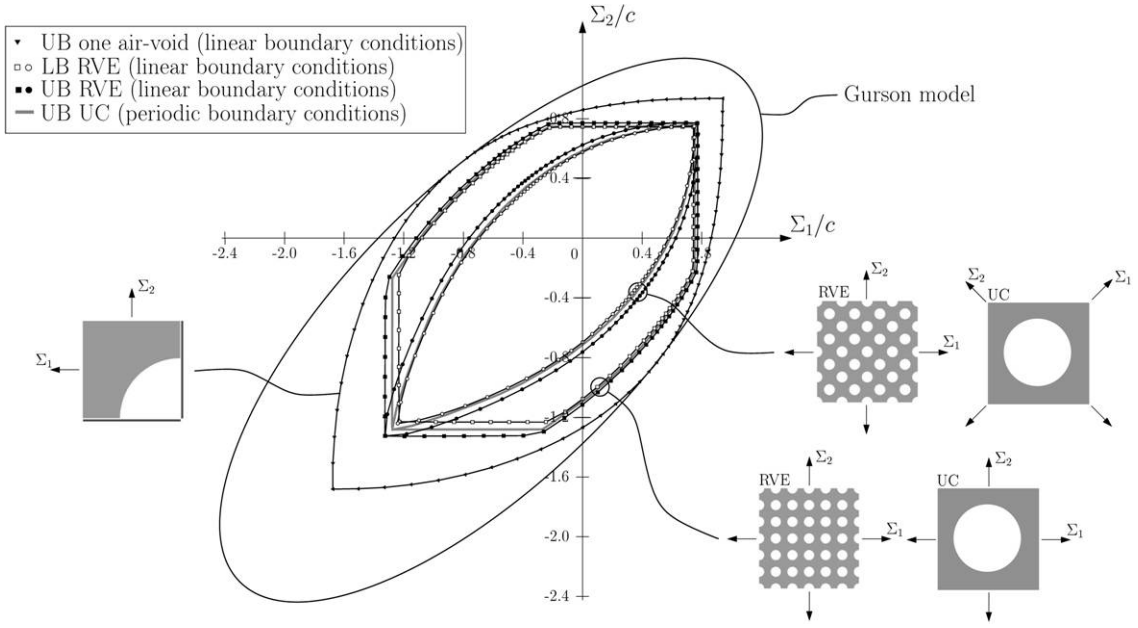

Figure 1: UB and LB of 2D effective yield surfaces (plane-strain situation) compared with the result from the 2D Gurson model ($f_a=30\%$, matrix material: Mohr-Coulomb with $c=10$ Pa and $\varphi=10^\circ$)

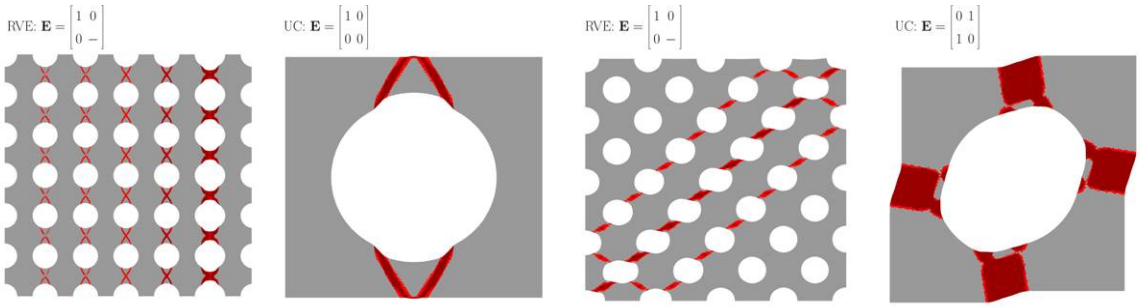

Figure 2: Comparison of failure modes obtained from RVE and UC approach for a porous material with $f_a = 30\%$ (matrix material: Mohr-Coulomb with $c = 10$ Pa, and $\varphi = 10^\circ$)

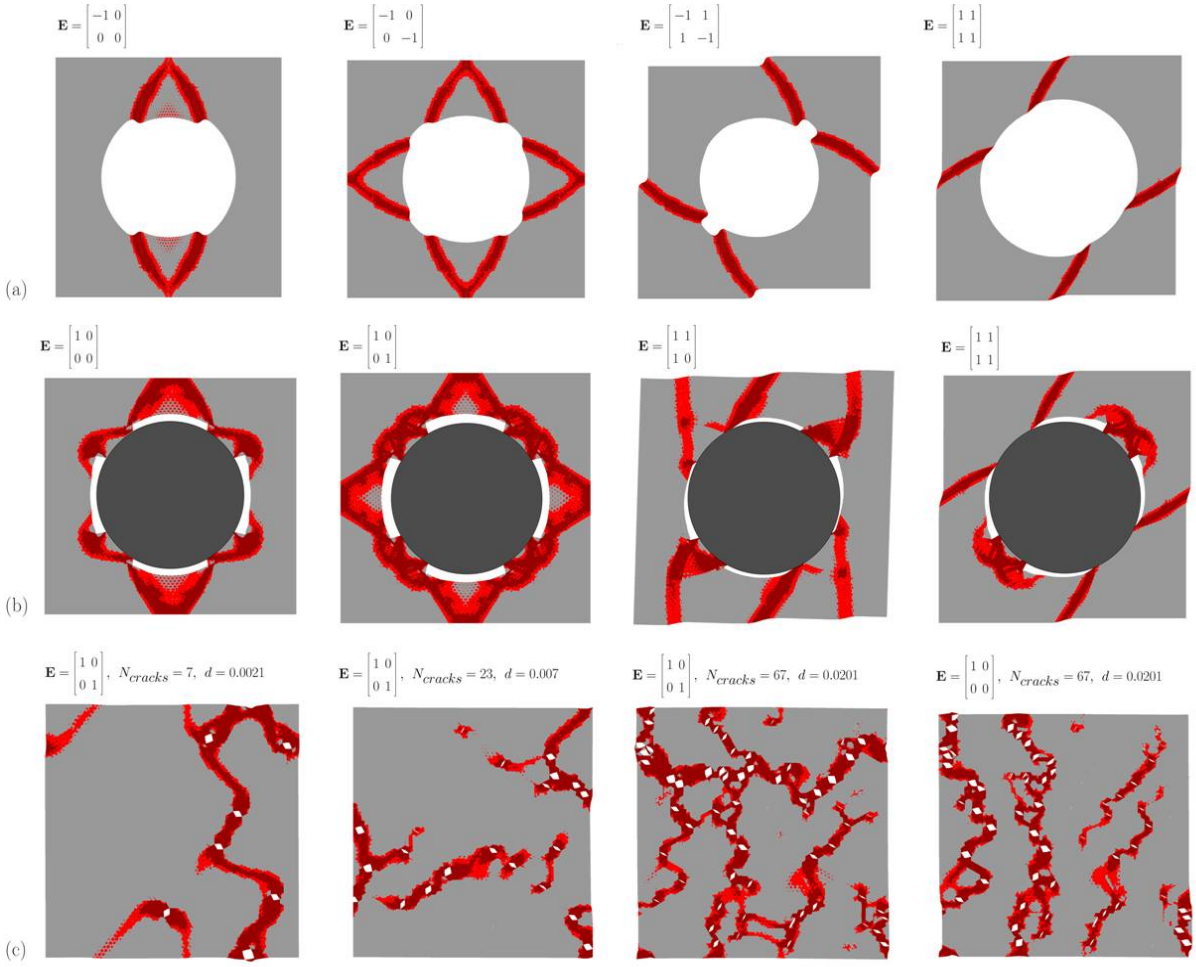

Figure 3: UB failure modes for different two-phase materials obtained from (a,b) UC approach (periodic boundary conditions) and (c) RVE approach (periodic boundary conditions) (matrix material: Mohr-Coulomb with $c = 10$ Pa, and $\varphi = 10^\circ$, 'rigid' particle)

The possibility of reducing/deactivating the strength of the interface allows consideration of debonding between particles and the matrix during upscaling. Finally, Figure 3(c) shows failure modes corresponding to different crack densities, defined by the dimensionless parameter $d = \sum_{N_{\text{cracks}}} (\text{crack length})^2 / (\text{area of RVE})$. Hereby,

the failure mechanism is composed by plastic failure zones developing between the existing (prescribed) microcracks, with the latter strongly affecting the failure mechanism.

2.2 3D matrix-inclusion materials

In this subsection, two-phase materials, consisting of particles (index "p") surrounded by a matrix (index "m"), and the interface (index "i") between them, are investigated (see Figure 3(a)). For the mechanical description of the matrix, the particles, and the interfaces, the Drucker-Prager failure criterion is employed, with *a* and *k* characterizing the internal friction angle and the limit in pure shear, respectively. By varying the loading situation Σ on the considered volume element of the material, microstructure-based effective failure criteria are derived for different material compositions (see Figures 3(b) and (c)). Figure 3(b) shows the effective failure surface for different particle contents f_p in the deviatoric plane for $\Sigma_m = 0$. As a result of the particle, the rotational symmetry of the Drucker-Prager failure surface assigned to the matrix material is lost. Macroscopic stress states characterized by a Lode angle $\vartheta = 60^\circ$ (compressive meridian) lead to a higher material strength than stress states located on the tensile meridian (Lode angle $\vartheta = 0^\circ$). This out-of-roundness effect increases with increasing particle content and decreasing mean stress (see Figures 3(b) and (c)). In the deviatoric plane, the resulting failure surface can be approximated with three ellipses, which is consistent with experimental data for different matrix-particle materials. For the case of a non-perfect bond between the matrix and the particle, a thin interface zone is considered in the volume element, with the strength properties a_I and k_I. Figure 3(c) shows upper bounds for the 3D failure surface of a matrix-particle material with degraded and non-degraded interface, respectively. For positive mean stress Σ_m, the material strength becomes lower than the strength of the pure matrix material. The largest reduction of the material strength (about 50%) is obtained for pure hydrostatic tensile loading.

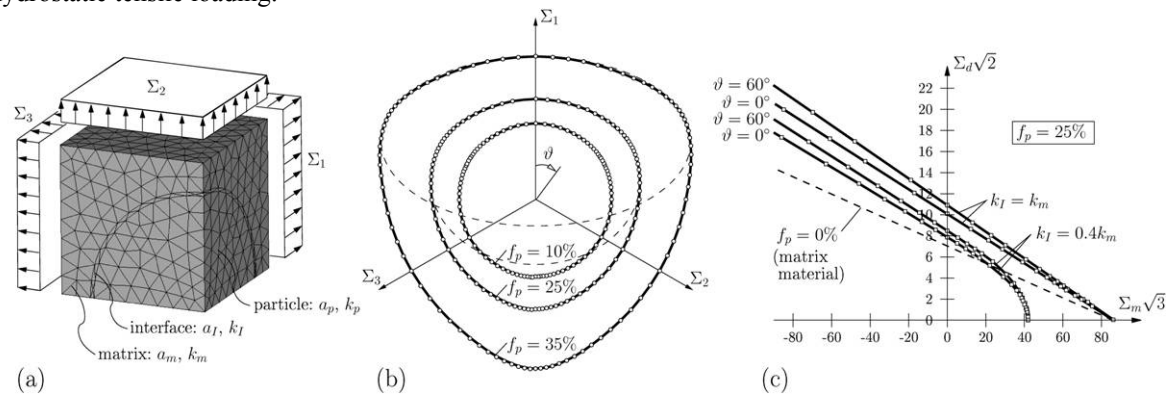

Figure 3: (a) Discretization of the considered volume element for the application of the UB theorem (one particle, linear boundary conditions), (b) UB of effective failure surface in deviatoric plane at $\Sigma_m = 0$ for different particle contents f_p (rigid particle), and (c) influence of degraded interface ($a_I = a_m$, $k_I = 0.4\,k_m$) on UB of the effective failure surface ($f_p = 25\%$, $a_m = 0.1$, $k_m = 5$)

References

[1] Füssl J, Lackner R, Eberhardsteiner J, Mang HA. Failure modes and effective strength of two-phase materials determined by means of numerical limit analysis. *Acta Mechanica* 2008; **195**(1-4): 185-202.

[2] Lyamin AV, Sloan SW. Lower bound limit analysis using non-linear programming. *International Journal for Numerical Methods in Engineering* 2002; **55**:573-611.

[3] Makrodimopoulos A and Martin CM. Limit analysis using large-scale SOCP optimization. In *Proc. 13th Nat. Conf. of UK Association for Computational Mechanics in Engineering,* Sheffield 2005; 21-24.

[4] Makrodimopoulos A and Martin CM. Lower bound limit analysis of cohesive-frictional materials using second-order cone programming. *International Journal for Numerical Methods in Engineering* 2006; **66**(4):604-634.

Proceedings of the 6th International Conference on
Computation of Shell and Spatial Structures
IASS-IACM 2008: "Spanning Nano to Mega"
28-31 May 2008, Cornell University, Ithaca, NY, USA
John F. ABEL and J. Robert COOKE (eds.)

Fracture analyses of fiber-reinforced concrete structures

John BOLANDER*

*Department of Civil and Environmental Engineering
University of California, Davis
Davis, CA 95616 USA
jebolander@ucdavis.edu

Abstract

Short fiber reinforcement is added to structural concrete to improve various aspects of the concrete, including its post-cracking strength and toughness. The degree of performance improvement is dependent on many factors, including the properties of each phase of the material (i.e., matrix, fiber, and matrix-fiber interface), fiber dosage, and the dispersion of fibers within the structural component. Computer modeling offers a precisely controlled environment for studying these factors and their interrelations.

This presentation concerns the development and validation of three-dimensional lattice models of fiber-reinforced concrete, in which the pre- and post-cracking actions of individual fibers are explicitly modeled. For most any practical situation, however, the number of fibers is large so that computational expense can become an issue. A basic example is presented to demonstrate the effects of fiber distribution on post-cracking strength and toughness. The importance of processing techniques becomes more clearly evident, since regions of lower fiber content, or with unfavorable fiber alignments, act as flaws and weaken the composite material.

1. Introduction

Concrete is a quasi-brittle material with limited post-peak load carrying capacity in tension. With appropriate additions of short fibers, the tensile performance is greatly improved due to additional toughening and strengthening mechanisms, including the arrest of macro- and/or microcracks, frictional pullout of the fibers, and fiber plasticity (in the case of metallic fibers). Successful applications of fiber-reinforced cement composites (FRCC) depend on material composition and the methods of processing. In particular, the dispersion and orientation of fibers within a structural element can strongly affect crack formation and growth, and the ensuing failure processes under continued loading. Crack widths and spacing are known to be important indicators of the durability of structural concrete, particularly with exposure to harsh environments. This paper describes a three-dimensional lattice model of FRCC fracture, in which each fiber is explicitly represented within the structural domain.

2. Lattice model of FRCC

2.1 Matrix phase

The matrix phase of the FRCC is assumed to be homogeneous and is modeled as a Rigid-Body-Spring Network, which is a type of lattice model. The lattice is constructed on a set of nodes placed in the structural domain using pseudo-random numbers. The lattice topology is based on the Delaunay tessellation of this point set, whereas the properties of the lattice elements are based on the dual Voronoi tessellation of the same point set. Procedures for discretization, and the formulations for elasticity and fracture analyses, are described elsewhere (Bolander and Saito, 1998; Yip *et al*., 2006).

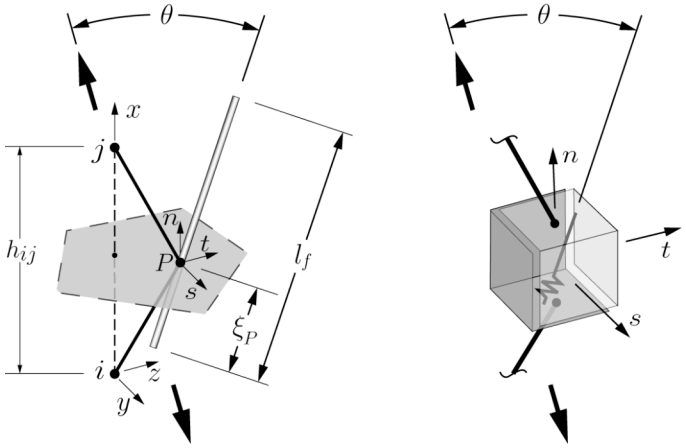

Figure 1: Fiber element *ij*

2.2 Fiber inclusions

Fibers are placed in the structural domain using pseudo-random numbers. If a fiber intersects the Voronoi facet associated with nodes *i* and *j*, then it contributes to the stiffness terms associated with those two nodes. The concept is illustrated in Fig. 1, where a fiber of length l_f crosses a Voronoi facet at point *P*. A zero-length spring is positioned at point *P* and aligned in the fiber direction; θ is the angle between the fiber longitudinal axis and the prevailing load direction. Prior to matrix cracking, the stiffness of this spring is based on elastic shear lag theory. After cracking of the matrix element associated with nodes *i* and *j*, the spring stiffness accounts for the mechanics of debonding and frictional slip of the fiber-matrix interface. The spring ends are connected to the nodal degrees of freedom via rigid arms *iP* and *jP*, as shown in the figure. Li *et al*. (2006) provide further details on the formulation of the fiber element.

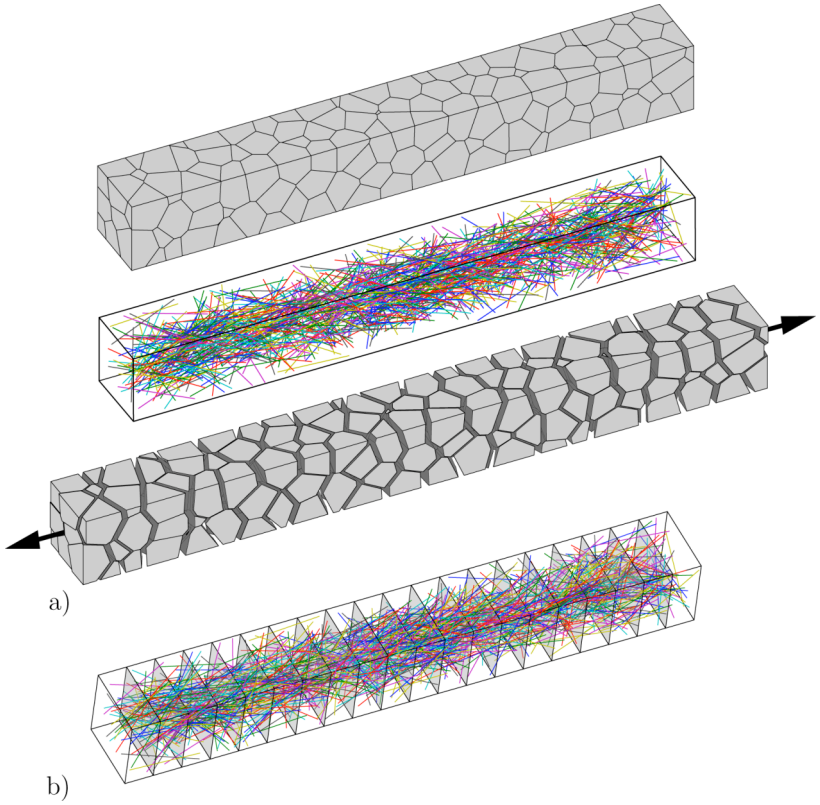

Figure 2: a) Irregular lattice model of FRCC specimen; b) regular discretization of nominally identical specimen

3. Simulation of uniaxial tension test

Tensile loading of a prism of dimensions 8*D*x*D*x*D* is simulated using the lattice model shown in Fig. 2a. The volume fraction of fibers is 1%, the fiber length is *D*, and the fiber aspect ratio is $l_f/d_f = 100$, where d_f is the fiber diameter. Prior to matrix cracking, the simulated elastic modulus of the composite differs from mixture rule predictions by only 0.2%, where the mixture rule accounts for length and orientation efficiency factors of the fibers (Bolander and Duddukuri, 2008).

As a first step in studying the fracture properties of FRCC, the simpler mesh shown in Fig. 2b is used. Figure 3 shows the tensile load-displacement response for several different bond strengths τ_f of the fiber-matrix interface; P_{cr} is the cracking load of an unreinforced prism. Cracking occurs where the matrix stress is the highest (which corresponds to where the efficiency of fiber reinforcement is the least). With increasing bond strength, the post-cracking strength and toughness increase. For sufficiently high bond strength, the post-cracking strength is greater than the first cracking strength so that multiple cracking occurs.

Figure 4 presents the *P*-δ response for 12 random realizations of the fiber distribution. There is significant scatter in composite strength, despite the usage of pseudo-random numbers to set the fiber end coordinates. Localization and complete pullout occur at the section with the smallest average embedment length, which generally differs from the section of first cracking.

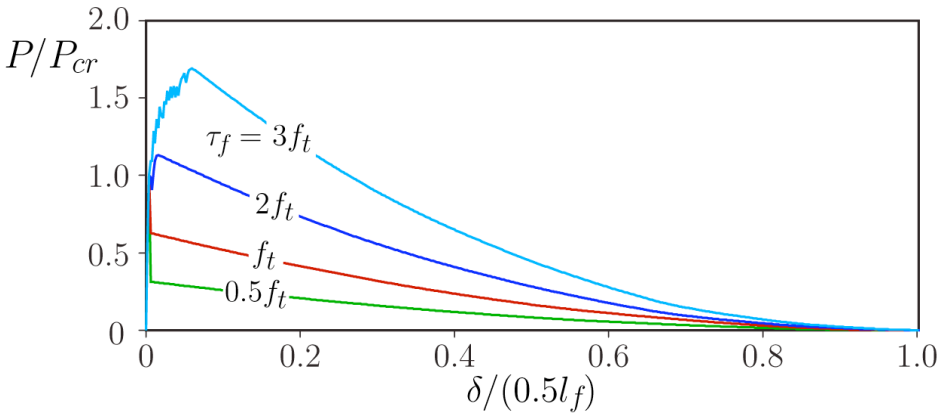

Figure 3: Effect of interfacial bond strength on tensile response

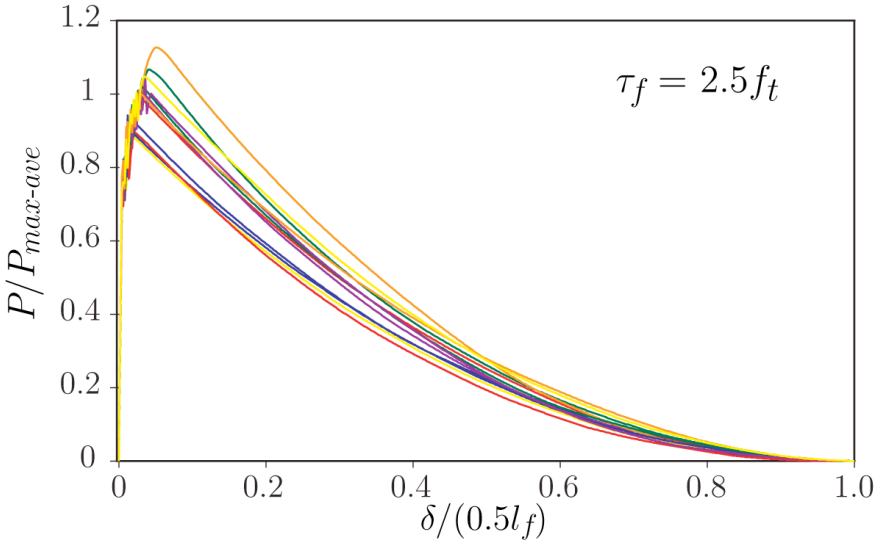

Figure 4: Effect of fiber distribution non-uniformity on tensile response

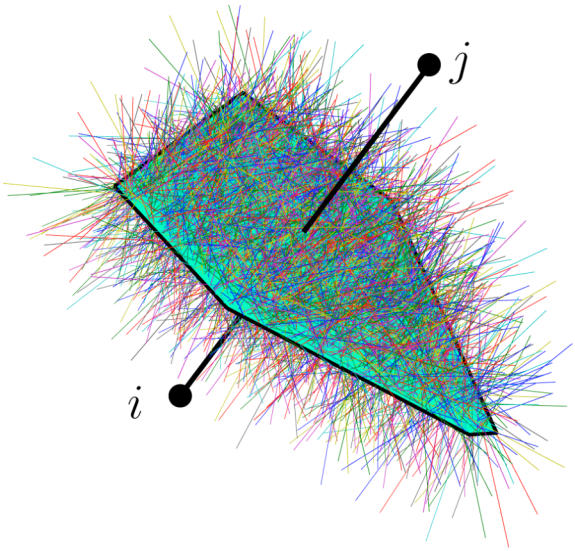

Figure 5: Microfibers intersecting Voronoi facet associated with nodes *i* and *j*

4. Summary

A lattice model is being developed to simulate fracture of fiber-reinforced cement composites. One distinguishing feature of the model is the explicit representation of each fiber in the structural domain. This is advantageous, since it enables a direct accounting of the effects of fiber distribution on post-cracking strength and toughness, as demonstrated through a simple example in which the matrix phase was coarsely discretized. Ultimately, finer discretizations are needed to study some important topics, such as the pinning of microcracks with highly dispersed microfibers. Analyses of micro-fiber composites are possible (Fig. 5), since fiber additions do not increase the number of degrees of freedom of the system (Bolander and Duddukuri, 2008).

Acknowledgement

The contributions of MS degree students Sri Ramya Duddukuri and Ji Cheng Kim are gratefully acknowledged.

References

[1] Bolander JE, Duddukuri SR. Effects of fiber type and dispersion on FRCC cracking potential. In *CCEDS-II: Sustainability of Civil Engineering Structures*, Chidiac S (ed.), McMaster University, Ontario, Canada, 2008 (to appear).

[2] Bolander JE, Saito S. Fracture analysis using spring networks with random geometry. *Engineering Fracture Mechanics* 1998; 61: 569-591.

[3] Li Z, Perez Lara M, Bolander JE. Restraining effects of fibers during non-uniform drying of cement composites. *Cement and Concrete Research* 2006; **36**(9): 1643-1652.

[4] Yip M, Li Z, Liao B-S, Bolander JE. Irregular lattice models of fracture of multiphase particulate materials. *International Journal of Fracture* 2006; **140**(1-4): 113-124.

Proceedings of the 6th International Conference on
Computation of Shell and Spatial Structures
IASSM-IACM 2008: "Spanning Nano to Mega"
28-31 May 2008, Cornell University, Ithaca, NY, USA
John, F. ABEL and Robert COOKE (eds.)

Crack-centered enrichment for debonding in two-phase composite applied to textile reinforced concrete

Rostislav Chudoba*, Jakub Jeřábek, Frank Peiffer and Joseph Hegger

* Institute of Structural Concrete
RWTH Aachen, Germany
Mies-van-der-Rohe-Str. 1, 52074 Aachen
rch@lbb.rwth-aachen.de

Abstract

Textile reinforced concrete (TRC) is a composite material combining the advantages of fiber reinforced concrete and steel reinforced concrete. Textile fabrics made out of glass, carbon or aramid are embedded in a cementitious matrix. In this work, the eXtended Finite Element Method (XFEM) is utilized to reflect the local displacement fields in the vicinity of crack bridges. The standard finite elements are augmented with special functions reflecting the discontinuities both in the matrix displacement and in the slip between the matrix and the reinforcement. The approach is presented on 1D example of a tension bar and a 2D analysis of shear zones with a detailed approximation of the local deformation fields in the crack bridge.

1 Introduction

Special effects in the load-bearing behavior of textile-reinforced cementitious composites occur due to the fact that the heterogeneity of both the matrix and the reinforcement occur at similar length scales of the material structure. This fact is particularly important in the post-cracking regime where the crack bridges develop to hot spots of textile damage. Therefore, one of the key prerequisites for reliable prediction of load-carrying capacity is a detailed representation of the crack bridge state in terms of the crack opening and crack sliding.

The XFEM provides an elegant tool for introducing discontinuities and material interfaces into an originally smooth discretization [1] independent of the initial mesh. In the approach presented here, we extend the discontinuity enrichment by an explicit representation of the debonding between the matrix and the reinforcement. The variational framework is established using a two-layered body occupying the domain Ω with the boundary Γ. The resolution of the material components into separate layers is introduced adaptively together with the propagation of cracks. One layer represents the cracking matrix, the other one the reinforcement (see Figure 1a). Once a crack gets introduced into the matrix using the XFEM enrichment the discretization in the vicinity of the crack gets adapted such that the slip between the two layers can develop. The interface behavior is governed by a general debonding law.

2 Displacement enrichment

The displacement resolution can be constructed in several ways that we classify into global and crack-centered (smooth or rough) approaches. In order to device a an efficient and targetted solution strategy with a potential to zoom into the micro-structure at the crack bridges we focus on the crack-centered approach here.

For a special case of a purely frictional bond (constant shear flow $\tau(s)$ for arbitrary value of slip s) and one-dimensional problem, analytical solution of the debonding can be found leading to a smooth approximation of the separate displacement fields. However, in a general case of an arbitrary bond law and for two-dimensional problems a numerical approach has to be chosen. Then, the crack-centered (rough) enrichment is realized using fine scale enrichment for the debonding over the range $x \in \Omega_a$ (Figure 1a). The displacement fields $\boldsymbol{u} = \{u_\mathrm{m}, u_\mathrm{f}\}^T$ of the matrix and filaments are expressed in the form:

$$\left[\begin{array}{c} u_\mathrm{m} \\ u_\mathrm{f} \end{array}\right] = \left[\begin{array}{c} u_\mathrm{s} \\ u_\mathrm{s} \end{array}\right] + \left[\begin{array}{c} \tilde{u}_\mathrm{m}^{(\xi)} \\ \tilde{u}_\mathrm{f}^{(\xi)} \end{array}\right] \quad \text{or} \quad \boldsymbol{u} = \boldsymbol{I} u_\mathrm{s} + \tilde{\boldsymbol{u}}_\mathrm{a}^{(\xi)} \tag{1}$$

where $\boldsymbol{I} = [1,1]^T$, u_s represents the effective global displacements shared by both matrix and reinforcement displacement fields and $\tilde{\boldsymbol{u}}_\mathrm{a} = \{\tilde{u}_\mathrm{m}, \tilde{u}_\mathrm{f}\}^T$ contains the local deviations from the global field.

The global field u_s is constructed with the goal to reflect the effective behavior of the composite. This field provides sufficient displacement representation in zones without debonding, i.e. without local effects. Standard polynomial shape function are used in the approximation of the global field.

$$u_\mathrm{s} = \boldsymbol{N}_\mathrm{s} \boldsymbol{d}_\mathrm{s} \tag{2}$$

The local fields $\tilde{\boldsymbol{u}}_\mathrm{a}$ reflect the matrix crack and the debonding process explicitly in the displacement approximation. This is done by using the XFEM method for the crack and additional polynomial shape functions on a local mesh covering the debonded domain Ω_a. The local discretization becomes

$$\tilde{\boldsymbol{u}}_\mathrm{a}^{(\xi)} = \boldsymbol{I} \boldsymbol{N}_\mathrm{s} \Psi^{(\xi)} \boldsymbol{d}_\psi^{(\xi)} + \boldsymbol{N}_\mathrm{a}^{(\xi)} \boldsymbol{d}_\mathrm{a}^{(\xi)}. \tag{3}$$

Here, the XFEM enrichment is constructed with respect to an enriched node j as

$$\Psi_j^{(\xi)}(x) = \mathrm{sign}(\Phi^{(\xi)}(x)) - \mathrm{sign}(\Phi^{(\xi)}(x_j)) \tag{4}$$

with $\Phi^{(\xi)}$ denoting the level set function $\Phi^{(\xi)}(x_\xi) = 0$.

In order to reflect the local deviations of the matrix and fiber displacement, we introduce crack centered shape functions $\boldsymbol{N}_\mathrm{a}^{(\xi)}$ defined on a local mesh covering $\Omega_\mathrm{a}^{(\xi)}$. For one-dimensional problems the enriched domain is defined as

$$\Omega_\mathrm{a}^{(\xi)} = \{x \mid R > |x - x_\xi|\} \tag{5}$$

where R denotes the maximum anticipated debonding distance from the crack x_ξ. In general, the local shape functions should be selected with a higher polynomial degree than the standard mesh. In the following we assume a linear approximation of the global standard approximation and quadratic polynomials for the local enrichment functions (see Figures 1b and 1c)

$$\boldsymbol{N}_\mathrm{a}^{(\xi)} = \left[\begin{array}{cc} \boldsymbol{N}_\mathrm{m}^{(\xi)} & \boldsymbol{0} \\ \boldsymbol{0} & \boldsymbol{N}_\mathrm{f}^{(\xi)} \end{array}\right], \quad \boldsymbol{d}_\mathrm{a} = \left\{\begin{array}{c} \boldsymbol{d}_\mathrm{m}^{(\xi)} \\ \boldsymbol{d}_\mathrm{f}^{(\xi)} \end{array}\right\}. \tag{6}$$

The shape functions used for the matrix and reinforcement fields $\boldsymbol{N}_\mathrm{m}^{(\xi)}$ and $\boldsymbol{N}_\mathrm{f}^{(\xi)}$ are equal. Furthermore, the debonding process is independent at both sides of the crack:

$$\boldsymbol{N}_\mathrm{m}^{(\xi)} = \boldsymbol{N}_\mathrm{f}^{(\xi)} = \left[\begin{array}{cc} \boldsymbol{N}^{(\xi-)} & \boldsymbol{N}^{(\xi+)} \end{array}\right] \tag{7}$$

where $^{(\xi-)}$ and $^{(\xi+)}$ stand for $\Phi^{(\xi)}(x) < 0$ and $\Phi^{(\xi)}(x) > 0$, respectively, i.e. for the two sides of a crack. The shape functions $\boldsymbol{N}^{(\xi\pm)}$ constitute the polynomial approximation of the debonding on the local mesh on both sides of a crack ξ (comp. Figures 1).

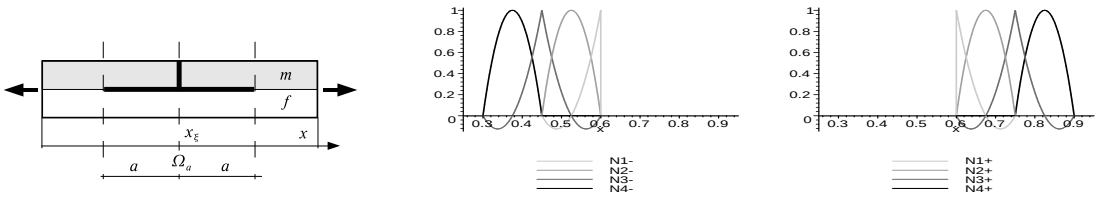

(a) Crack bridge resolution (b) Shape functions $\boldsymbol{N}^{(\xi-)}$ (c) Shape functions $\boldsymbol{N}^{(\xi+)}$

Figure 1: Debonding enrichment for a single crack ($x_\xi = 0.6$, $R = 0.3$, $n_a = 2$ enrichment elements).

3 Continuity constraint

The enrichments for both sides of the crack are completely decoupled i.e. they do not share degrees of freedom at the crack bridge position. As a consequence, the given discretization is not in compliance with the continuity condition imposed on the reinforcement displacement field. Instead, as shown in Figure 2a there are jumps both in the XFEM part and in the independent local enrichments (from the left and the right of the crack). The continuity can be recovered by imposing the requirement that the sum of the two jumps in the displacement at x_ξ must be zero

$$[\![\tilde{u}_\mathrm{f}]\!]_\xi = 2\boldsymbol{N}_\mathrm{s}(x_\xi)\boldsymbol{d}_\psi^{(\xi)} + \boldsymbol{N}_\mathrm{f}^{(\xi)}(x_\xi)\boldsymbol{d}_\mathrm{f}^{(\xi)} = 0. \tag{8}$$

By applying Eq. (8) as a kinematic constraint we can eliminate one degree of freedom associated with the jump as

$$d_{\mathrm{f},1}^{(\xi-)} = d_{\mathrm{f},1}^{(\xi+)} + 2\boldsymbol{N}_\mathrm{s}(x_\xi)\boldsymbol{d}_\psi^{(\xi)} \tag{9}$$

where $d_{\mathrm{f},1}^{(\xi-)}$ and $d_{\mathrm{f},1}^{(\xi+)}$ represent the fiber displacements at either side of the crack. This constraint gets integrated into the shape functions (3) so that the continuity of the shape functions gets recovered as shown in Figure 2b.

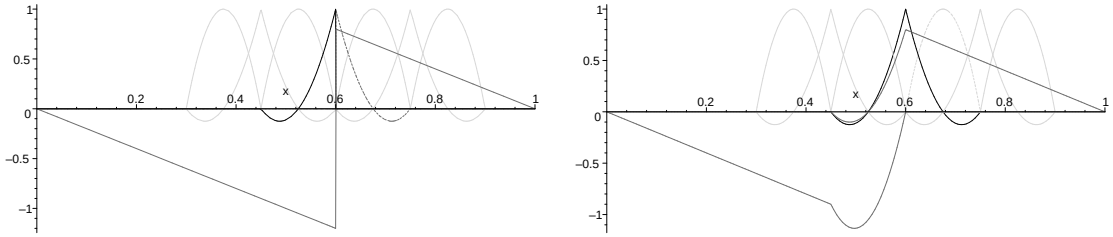

(a) Unconstrained functions. The four functions with jumps are shown in black.

(b) Continuous functions with kinematic constraint. Affected functions are shown in black.

Figure 2: Integration of the kinematic constraint into the approximation of the reinforcement displacement ($x_\xi = 0.6$, $R = 0.3$).

4 Variational formulation

The local equilibrium in the vicinity of the crack bridge over an unknown debonded length a is varied with respect to the virtual local fields $\delta\tilde{u}_m$, $\delta\tilde{u}_f$:

$$\begin{aligned} (\delta\tilde{u}_m, [E_m u_{,xx} + E_m\tilde{u}_{m,xx} + \tau])_{\Omega_a} &= 0 \\ (\delta\tilde{u}_f, [E_f u_{,xx} + E_f\tilde{u}_{f,xx} - \tau])_{\Omega_a} &= 0 \end{aligned} \tag{10}$$

where $(-,-)_{\Omega_a}$ denotes integration over the range $x_\xi \pm a$. The previously introduced displacement approximation together with the corresponding constitutive expressions for the matrix, reinforcement and

their bond must be plugged in into the variational formulation. The derivation falls within the multiscale variational framework [2]. The resulting discrete equilibrium equations are generally non-linear and must be solved incrementally.

5 Examples

Figure 3a shows the solution of a uni-axially loaded crack bridge in the form of displacement and stress profiles. The stress profile of the matrix shows that the approximation is able to reproduce zero matrix stress at the position of the crack bridge.

As mentioned in the beginning, the development of this approach is motivated by the need for high-quality resolution of the shear zones in the simulation of bending specimens and connection details. These cases exhibit relatively coarse crack pattern. An example of a calculated strain field in the matrix is shown in Figure 3b. The hot spots of reinforcement damage are encountered in the vicinity of dominating cracks. Therefore, the quantification of the crack opening and crack sliding displacement is of crucial importance to assess the state of the damage in the bond. The presentation will provide a comparison between the local, crack-centered enrichment and global bond discretization on the example of experimentally traced shear zones of TRC bending specimens.

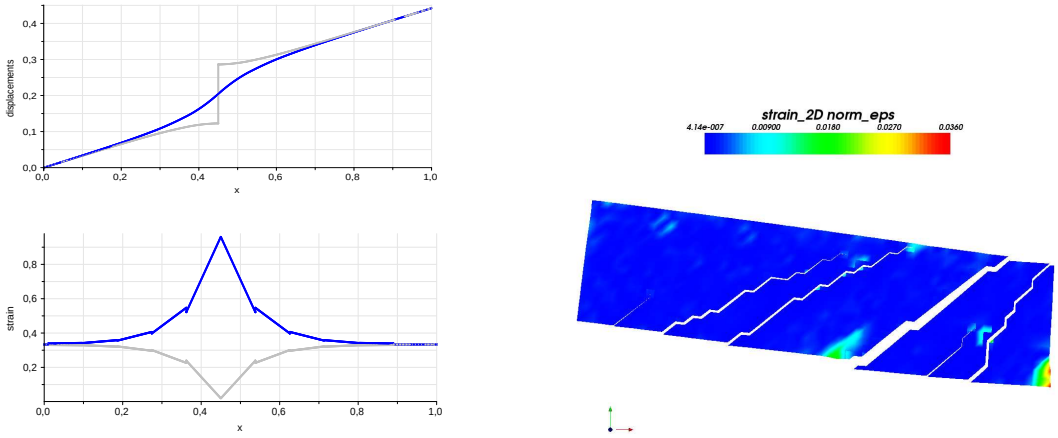

(a) Example of a single crack bridge (displacement and stress in the matrix and in the reinforcement)

(b) Example of a shear zone of a TRC specimen (strain distribution in the matrix)

Figure 3: Demonstrative example 1D example (left) and application to the shear zone (right)

Acknowledgment

The present work has been carried out in the framework of the project *Numerical modeling of textile-reinforced concrete at the meso-level* included in the collaborative research center *Textile reinforced concrete: foundation of a new technology (SFB 532)* sponsored by the German Research Foundation.

References

[1] Belytschko T., Moës N., Usui S., and Parimi C. Arbitrary discontinuities in finite elements. *International Journal for Numerical Methods in Engineering* 2001; **50**

[2] Hughes, T.J.R and Feij, G.R. Mazzei and L. Quincy, J.B.. The variational multiscale method: a paradigm for computational mechanics. *Computer Methods in Applied Mechanics and Engineering* 1998; **166**:3-24

Proceedings of the 6th International Conference on
Computation of Shell and Spatial Structures
IASS-IACM 2008: "Spanning Nano to Mega"
28-31 May 2008, Cornell University, Ithaca, NY, USA
John F. ABEL and J. Robert COOKE (eds.)

Three-dimensional higher order X-FEM model for multifield durability and failure analysis of concrete structures

Stefan JOX, Christian BECKER, Günther MESCHKE*

*Institute for Structural Mechanics, Ruhr University Bochum
Universitätsstr. 150, D-44801 Bochum, Germany
{stefan.jox,guenther.meschke}@rub.de

Abstract

This paper is concerned with a spatial and temporal discretization concept specifically designed for durability oriented computational analyses of concrete structures with specific emphasis on the interactions between cracks and the transport of moisture relevant for the long-term degradation of concrete structures. The proposed concept combines a hierarchically organized p-finite element formulation for the discretization of the continuous fields (displacements, capillary pressure) with the X-FEM [1] for the discrete representation of cracks. To this end, a coupled hygro-mechanical model formulated in the framework of the BIOT-COUSSY-Theory is incorporated into the higher order X-FEM simulation strategy. The performance of the proposed discretization concept is demonstrated by means of 2D and 3D numerical examples, including mechanical and hygro-mechancial analyses.

1 Introduction

Lifetime-oriented analyses of concrete and reinforced concrete structures need to consider the accumulation of damage induced by time variant external loading as well as long term deterioration caused by environmental loading processes such as moisture and heat transport, freeze-thaw action, chemical dissolution and expansion reactions and the corrosion of the reinforcement. What makes such analyses particularly complex are the various interactions between the mentioned deterioration mechanisms. Multiphase material models formulated in the framework of the Theory of Porous Media have shown to be suitable to take interactions between individual phases and various processes acting on different spatial scales into account (see, e.g. [5]). The presented paper focusses on spatial discretization techniques characterized by a higher order finite element formulation (p-FEM) combined with the Extended Finite Element Method (X-FEM) specifically designed for durability oriented computational analyses of concrete structures with emphasis on the interactions between (loading induced) cracks and the transport of moisture relevant for the long-term degradation of concrete structures.

2 Hygro-mechanical model and moisture transport

In the proposed model, full coupling between moisture transport and the mechanical behaviour of concrete is taken into account in the framework of the BIOT-COUSSY theory [6]. The presence of moisture fields may lead to crack initiation (e.g., in restrained drying processes) and, conversely, cracks strongly affect the permeability of the material. In this paper both a continuous and a discontinuous numerical representation of hygro-mechanical couplings are considered. In the continuum-based formulated hygro-mechanical material model, cracking of concrete is accounted for by an anisotropic plasticity-damage model, see e.g. [7], in which the concept of effective plastic stresses is used and the crack width is related to the internal variable α_R of the Rankine yield surface [6]. Within

the discontinuous concept, cracks are represented by a displacement discontinuity by means of the X-FEM (see Section 4).

According to the coupled two-phase model, the total stresses $\boldsymbol{\sigma}$ depend on the effective matrix stresses $\boldsymbol{\sigma}'$, the capillary pressure p_c and the capillary-pressure relation $S_l(p_c)$. Moisture flow in the intact parts of the material is modelled by a diffusion law, whereas the moisture flux along one single crack is modeled by the NAVIER-STOKES equation (POISEUILLE flow, crack width w) characterized by the permeabilities

$$\mathbf{k}_{por} \;=\; k_\phi(\phi)\,\mathbf{k}_f(S_l) \quad \text{and} \quad k^t_{cr} \;=\; k_{rc}(S_l)\,k^t_{cr0}(w) \tag{1}$$

taking the dependency of the liquid saturation S_l and the porosity ϕ into account.

3 3D higher-order spatial discretization concept

The coupled differential equations of balance of momentum and balance of mass are discretized in time by means of an implicit finite difference method and integrated to the semi-discrete weak form of the coupled differential equations [4]. The weak form is spatially discretized using higher-order hierarchically organized LEGENDRE polynomials $P_n(\xi)$ generated by BONNET's recursion formula. Modified LEGENDRE polynomials $\Phi_i(\xi)$ serve as shape functions. Using anisotropic approximation spaces the higher order discretization strategy allows for the specific adaption of the approximaton to the required kinematics of the type of investigated structure (truss, beam, slab, plate, shell), leading, in the sense of [2], to *truss-like* solid ($\boldsymbol{u}_{p,1,1}$), *slab-like* solid ($\boldsymbol{u}_{p,p,1}$) or *shell-like* solid ($\boldsymbol{u}_{p,p,2}$, $\boldsymbol{u}_{p,p,3}$) formulations. Also the specific requirements of the individual fields (e.g. displacements, capillary pressure) can be well accomodated by a fieldwise choice of the hierarchical p-finite element formulation.

4 Three-dimensional X-FEM for hygro-mechanical analyses

Inserting the additive decomposition of the displacement field into a continuous and a discontinuous part

$$\boldsymbol{u}(\mathbf{X}) = \bar{\boldsymbol{u}}(\mathbf{X}) + \check{\boldsymbol{u}}(\mathbf{X}); \quad \check{\boldsymbol{u}}(\mathbf{X}) = S_S(\mathbf{X})\,\hat{\boldsymbol{u}}(\mathbf{X}) \tag{2}$$

into the weak form of balance of momentum leads to

$$\int_\Omega \delta\bar{\boldsymbol{\varepsilon}} : \boldsymbol{\sigma}\, dV + 2 \int_{\partial_S\Omega} \delta\hat{\boldsymbol{u}}\, \underbrace{\boldsymbol{\sigma}\,\boldsymbol{n}_S}_{\boldsymbol{t}_S}\, dA = \int_{\Gamma_\sigma} \delta\bar{\boldsymbol{u}}\,\boldsymbol{t}^\star\, d\Gamma_\sigma, \tag{3}$$

where $\delta\bar{\boldsymbol{\varepsilon}}$ includes the discontinuous part of the gradient of equation $(2)_2$ and $\boldsymbol{t}_S$ is the traction force acting on the discontinuity $\partial_S\Omega$. This traction force is directly related to the displacement jump $[\![\boldsymbol{u}]\!]$ through a softening traction-separation law $\boldsymbol{t}_S = \boldsymbol{t}_S([\![\boldsymbol{u}]\!])$ according to [9]. The present 3D implementation is characterized by an elementwise crack propagation of elementwise plane crack segments, a weighted principal stress criterion used for crack propagation and direction, a linear approximation of the enhanced displacement field associated with the crack opening in the element, a crack propagation algorithm relaxing the compatiblility reuqirements between crack segments [3]. For hygro-mechanically coupled problems, the weak formulation of linear balance of momentum is extended by

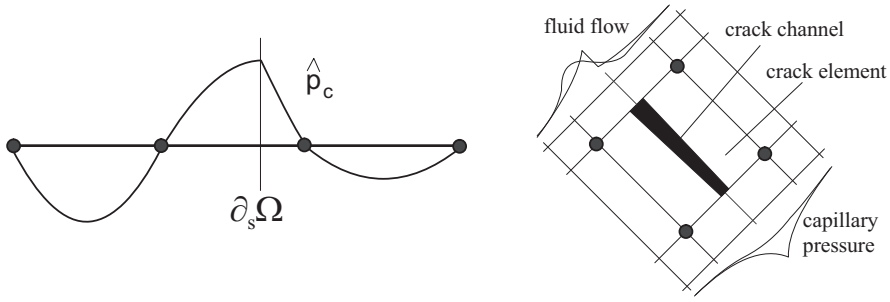

Figure 1: Enhancement of the capillary pressure field

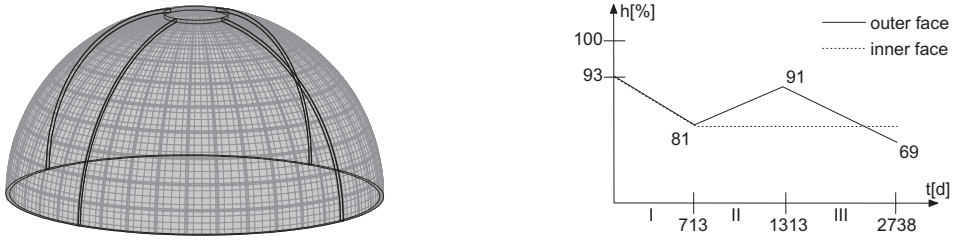

Figure 2: Concrete shell and hygral loading scenario

the balance of liquid mass

$$\int_{\Omega} \delta p_c \, \frac{\dot{m}_l}{\rho_l} \, dV \; - \int_{\Omega} \delta \nabla p_c \cdot \boldsymbol{q}_l \, dV \; = \int_{\Gamma_q} \delta p_c \, q_l^* \, dA. \tag{4}$$

In the context of hygro-mechanical analyses, the capillary pressure p_c can be approximated either C^0-continuous in an embedded formulation or C^1-continuous with the assumption of an interelemental discontinuous moisture flux normal to the crack channel [8], both taking the topology of the crack channel into account. The enhancement of the capillary pressure field (Fig. 1) results in additional nodal degrees of freedom

$$p_c \; = \; \bar{p}_c + \check{p}_c \quad \text{with} \quad \check{p}_c \approx \sum_{i=1}^{ns} N_i^{enh} \, \hat{p}_{ci}. \tag{5}$$

5 Hygro-mechanical analysis of a concrete shell

To illustrate the capability of the proposed higher-order finite element formulation a concrete shell ($E = 36700\,[N/mm^2]$, $\nu = 0.2$, $f_{tu} = 3.8\;[N/mm^2]$, $G_f = 0.169\;[N/m]$, radius $R = 5000\;[mm]$, thickness $t = 100\;[mm]$) subjected to hygro-mechanical loading is analyzed numerically (Fig. 2). The spatial discretization is chosen as $\boldsymbol{u} \approx \boldsymbol{u}_{3,3,4}, \quad p_c \approx p_{c\,2,2,3}$. Mechanical loading is represented by the dead load of the structure. The hygral loading (Figure 2) starts with a uniform drying of the inner and outer surface of the shell. The drying process initiates cracks opening at the outer surface of the shell which leads to an acceleration of the moisture transport (Fig. 3).

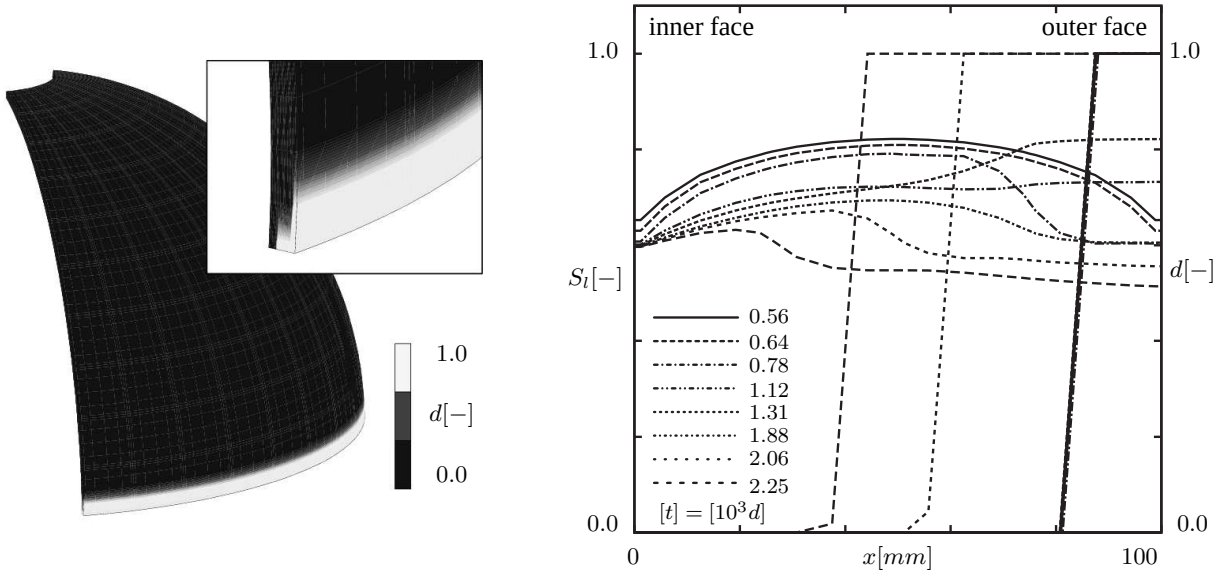

Figure 3: Analysis of a concrete shell: saturation and damage distribution through the thickness

6 Hygro-mechanically loaded concrete beam

A hygro-mechanical analysis of a concrete beam using the proposed higher order X-FEM model is perfomred next. Fig. 4 contains the geometry, the mechanical and hygral loading history and the spatial discretization ($\bar{\boldsymbol{u}}_{2,2,1}, p_{c\,1,1,1}$). After applying a displacement controlled point loading ($u^* = 0.56\,mm$) on the top of the beam, a drying process starting from the lower boundary Γ^2 where the initial saturation of $S_l^{*2} = 88.2\,\%$ ($p_c = 10.0\,N/mm^2$) is decreased to $S_l^{*2} = 58.8\,\%$ ($p_c = 20.0\,N/mm^2$) is simulated. Due to external loading a crack of $3.25\,mm$ opens at the bottom of the beam. The capillary pressure distribution illustrates the effect of the accelerated moisture transport through the crack after 40, 70, 100 and 130 hours.

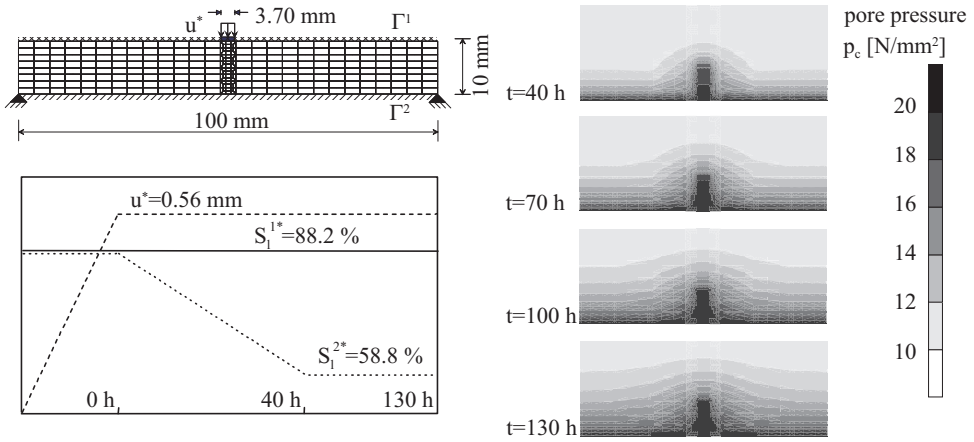

Figure 4: Hygro-mechanical analysis of a concrete beam

Acknowledgment

Financial support was provided by the German National Science Foundation (DFG) in the framework of project B3 of the collaborative research center (SFB) 398. This support is gratefully acknowledged.

References

[1] T. Belytschko and T. Black. Elastic crack growth in finite elements with minimal remeshing. *International Journal for Numerical Methods in Engineering*, 45:601–620, 1999.

[2] M. Bischoff and E. Ramm. Solid-like shell or shell-like solid formulation? A personal view. In A. Wunderlich, editor, *Proceedings of ECCM 99*, Munich, Germany, 1999.

[3] T.C. Gasser and G.A. Holzapfel. Modeling 3D crack propagation in unreinforced concrete using PUFEM. *Computer Methods in Applied Mechanics and Engineering*, 194:2859–2896, 2005.

[4] S. Jox, C. Becker, and G. Meschke. Hygro-mechanical coupled analyses of cracked cementitious materials in the framework of the extended finite element method. In A. Carpinetri et. al., editor, *FRAMCOS-6*, pages 517–524. Taylor & Francis, 2007.

[5] Ch. Leung, F. Ulm, Y. Xi, G. Pijaudier-Cabot, and S. Sture. Special topical issue on durability mechanics. *Journal of Engineering Mechanics (ASCE)*, 126(3):226–319, March 2000.

[6] G. Meschke and S. Grasberger. Numerical modelling of coupled hygro-mechanical degradation of cementitious materials. *Journal of Engineering Mechanics*, 129:383–392, 2003.

[7] G. Meschke, R. Lackner, and H.A. Mang. An anisotropic elastoplastic-damage model for plain concrete. *International Journal for Numerical Methods in Engineering*, 42:703–727, 1998.

[8] J. Rethore, R. de Borst, and M.-A. Abellan. A two-scale approach for fluid flow in fractured porous media. *IJNME*, 71:780–800, 2007.

[9] G.N. Wells and L.J. Sluys. Three-dimensional embedded discontinuity model for brittle fracture. *International Journal of Solids and Structures*, 38:897–913, 2001.

Proceedings of the 6th International Conference on
Computation of Shell and Spatial Structures
IASS-IACM 2008: "Spanning Nano to Mega"
28-31 May 2008, Cornell University, Ithaca, NY, USA
John F. ABEL and J. Robert COOKE (eds.)

From multi-scale to multi-grid FE analysis of concrete fracture

Chris J. PEARCE*, Łukasz KACZMARCZYK, Nenad BICANIC

*Department of Civil Engineering, The University of Glasgow, Glasgow G12 8LT, UK
pearce@civil.gla.ac.uk

Abstract

This paper sets out the basic ingredients for a two-grid approach for simulating fracturing in concrete where the fine scale heterogeneities are fully resolved. The very large system of algebraic equations that emerges from the detailed resolution requires an efficient iterative solver with a preconditioner that is appropriate for heterogeneous materials. This preconditioner is constructed using a two-grid strategy that utilizes scale transition techniques derived for computational homogenization. The performance of this preconditioner is illustrated on two numerical examples.

1. Introduction

The complex macroscopic behavior of many engineered and natural materials is rooted in the mechanics of the underlying heterogeneous microstructure. Multi-scale analysis techniques aim to capture this macroscopic behavior via the detailed modeling of the microstructure. Computational homogenization [1,2] is one such technique which utilizes nested multi-level finite element analyses, with discretisation on both the micro and macro levels and avoids the need for the full heterogeneous microstructure to be resolved. So-called first-order computational homogenization schemes do not take account of the microstructural length-scale and assume uniform macroscopic fields across the microstructure; thereby they are not able to capture microstructural geometric size effects and have limited applicability in areas with rapidly varying fields. The use of higher-order continua on the macro-scale and appropriate second-order homogenization schemes have been proposed [1,2,3] to deal with these issues. However, in situations involving the nucleation of defects into micro-cracks and coalescence into macro-cracks, homogenization procedures cannot be applied since micro-fluctuation fields are unbounded and representative volume elements cannot be constructed. Consequently, a computationally complex micro-scale analysis is required in which the heterogeneous microstructure is fully resolved.

The very large system of algebraic equations that emerges from the detailed resolution of the microstructure requires an efficient iterative solver and multi-grid techniques seem an appropriate choice. Miehe & Bayreuther [4] has presented a geometric multi-grid technique for solving problems with poor scale separation, with particular focus on heterogeneous nonlinear hardening materials in which the focus of attention is on the design of the geometric transfer operators. This paper develops a geometric second-order multi-grid approach as an extension of Miehe & Bayrether's work which is applicable to fracturing heterogeneous materials such as concrete. A second-order homogeneous continuum is assumed at the macro-scale and a classical continuum at the micro-scale. A hybrid-Trefftz stress element formulation [5,6] is utilized on the fine-scale for modeling propagating cohesive cracks. However, the focus of this abstract will not be on cohesive cracking but rather on the geometric transfer operators that are based on the scale transition algorithms developed for second-order computational homogenization.

2. Hybrid-Trefftz elements for fine scale modeling

A model for propagating cohesive cracks within the context of a hybrid-Trefftz formulation is utilised which is both robust and computationally efficient. The primary motivation was the development of a straightforward, accurate and robust model for cohesive cracking in heterogeneous materials where multiple cracks, crack branching and crack coalescence are the norm and where different constitutive models are required for the matrix, inclusions and interface. The formulation introduces discontinuities along element interfaces and this

normally requires displacement continuity to be enforced (before cracking occurs) via a high non-physical penalty-type stiffness which can result in an ill-conditioned system matrix. An alternative technique, based on the Uzawa method [7], which overcomes such problems is utilized here. One of the drawbacks of restricting discontinuities to element interfaces is the dependence of the solution on the underlying finite element mesh. This issue cannot be completely eradicated but can to a large extent be alleviated by ensuring that the mesh is randomly generated; this is typically achieved by using triangular elements. For classical displacement based finite elements, the simplest approximation basis for such elements results in overly stiff solutions and suffer from shear and volumetric locking. These issues are not relevant in the hybrid-Trefftz formulation presented here. Another advantage in adopting a hybrid-Trefftz formulation is that it leads to a sparse finite element system matrix that can be formulated using boundary rather than domain integrals [6]. The stress approximation is a priori constrained to satisfy the equilibrium condition locally and the boundary displacements are defined independently of the stresses.

3. Multi-grid preconditioner

Full resolution of the fine scale microstructure leads to a very large system of algebraic equations

$$\mathbf{K}^f \mathbf{d}^f = \mathbf{f}^f \tag{1}$$

and the solution of this system of equations requires an efficient iterative solver. Here a Krylov iterative solver is utilized that requires an appropriate preconditioner in order for the solver to be efficient and the fine-scale displacements are improved as

$$\mathbf{d}^f \leftarrow \mathbf{d}^f + \mathbf{B}\left(\mathbf{f}^f - \mathbf{K}^f \mathbf{d}^f\right) = \mathbf{d}^f + \mathbf{B}\mathbf{r}^f \tag{2}$$

where $\mathbf{r}^f$ is the fine scale residual and $\mathbf{B}$ is the preconditioner that is efficiently constructed here using a two-grid scheme. This is achieved by reducing the iteration defect on the fine scale using a stationary iterative method such as Gauss-Seidel with a limited number of iterations, thereby smoothing the short wave defect. The long wave component of the defect is smoothed by first restricting the residual onto a coarser grid

$$\mathbf{r}^c = \mathbf{P}^T \mathbf{r}^f \tag{3}$$

and then solving the following system of equations using a direct solver

$$\mathbf{K}^c \mathbf{z}^c = \mathbf{r}^c \tag{4}$$

where $\mathbf{K}^c = \mathbf{P}^T \mathbf{K}^f \mathbf{P}$ is the coarse scale system matrix. The resulting coarse scale defect is then prolongated back to the fine grid

$$\mathbf{z}^f = \mathbf{P}\mathbf{z}^c \tag{5}$$

The fine scale defect is then smoothed as before and the improved fine grid solution obtained as

$$\mathbf{d}^f \leftarrow \mathbf{d}^f + \mathbf{z}^f \tag{6}$$

The displacements prolongated from the coarse scale can be decomposed into long-wave and short wave contributions:

$$\mathbf{d}^f = \underbrace{\bar{\mathbf{d}}^f}_{\text{long-wave}} + \underbrace{\hat{\mathbf{d}}^f}_{\text{short-wave}} = \left(\bar{\mathbf{P}} + \hat{\mathbf{P}}\right)\mathbf{d}^c = \mathbf{P}\mathbf{d}^c \tag{7}$$

The long-wave displacements are associated with the homogeneous contribution of the coarse mesh approximation and the short-wave displacements represent fluctuations due to the fine-scale heterogeneous structure. Thus, it is possible to construct a transition operator $\mathbf{P}$ that is appropriate for heterogeneous materials using the scale transition techniques derived for computational homogenization.

4. C^1-continuous element for coarse scale modeling

In order to avoid mesh dependent solutions for heterogeneous quasi-brittle and softening materials, a gradient continuum is applied at the coarse scale that utilizes a C^1-continuous triangular element. This element has six degrees of freedom per vertex, i.e. two associated with displacements and four with the gradient of

displacements. The shape functions belong to Sobolev space H^2 and are adopted to develop an efficient, conformal finite element for second-order continuum. This element is a modification of a triangle element formulated in [8] for thin plates. The coarse mesh does not approximate heterogeneities, i.e. the characteristic size of coarse element is approximately one or two orders greater than the characteristic size of the fine scale structure. The coarse mesh associated with a gradient continuum enables higher-order boundary conditions to be taken into account, the long-wave defect to be smoothed and regularization of the problem when the fine-scale induces localization at the coarse-scale.

5. Numerical examples

5.1 Uniaxial test

In order to demonstrate the efficiency of the transfer operators between coarse and fine-scale meshes, a simple uniaxial problem with a heterogeneous microstructure is investigated. The coarse mesh comprises 16 C^1-continuous elements (Figure 1(a)) and the fine scale comprises 41669 triangular hybrid-Trefftz stress elements (Figure 1(b)). One end of the specimen is fixed horizontally and vertically and the other end is fixed vertically and a unit horizontal displacements prescribed. The material comprises strips of hard and soft material (Figure 1(c)), with $E_{\text{stiff}} = 10E_{\text{soft}}$ and $\nu = 0.25$. Figure 1(d) presents the exact distribution of stresses. The coarse scale problem is analysed and the displacement field is projected onto the fine scale using two types of boundary conditions, i.e. traction and displacement. Figure 2 shows the distribution of fine-scale displacement fluctuations and stresses respectively. It can be seen that the displacement fluctuations and the stresses correctly reflect the heterogeneous fine scale structure.

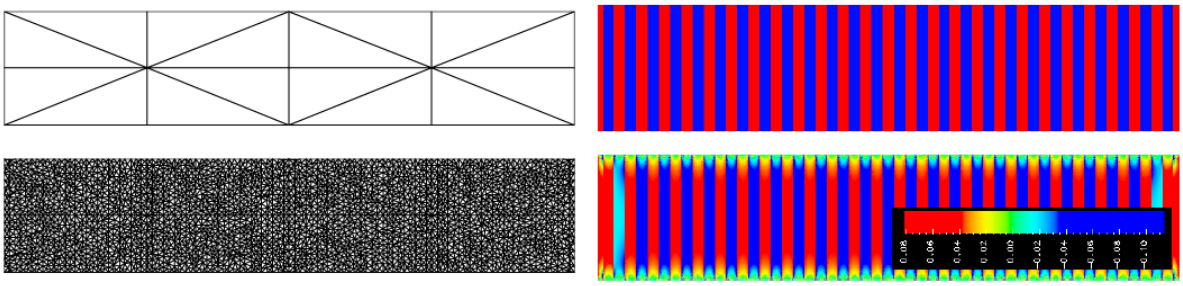

Figure 1: Uniaxial test. Left: coarse mesh and fine mesh. Right: distribution of soft (blue) and stiff (red) inclusions and exact distribution of σ_x.

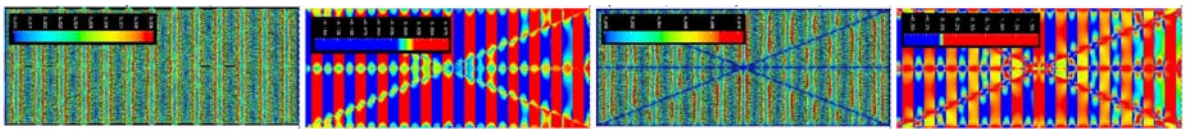

(a) (b) (c) (d)

Figure 2: Uniaxial test (half of specimen). Stress transfer operator: (a) fine-scale displacements, (b) fine-scale stresses. Displacement transfer operator: (c) fine-scale displacements, (d) fine-scale stresses.

5.1 Elastic heterogeneous specimen with a hole

An elastic heterogeneous specimen with a hole is discretised into both coarse-scale (1020 d.o.f.) and fine-scale (90436 d.o.f.) unstructured meshes (Figure 3). The quarter of the specimen under consideration has dimensions 10x10 with a hole radius of 1; a uniformly distributed normal tensile load $q = 1$ is applied along the right edge. In order to investigate the influence of the microstructure on the convergence of the proposed solution technique with multi-grid preconditioner, different microstructures are considered (Figure 3). The randomly distributed fibres have diameters of 0.05 and 0.1 with volume fractions of 0.1 and 0.05 repectively. Once again, $E_{\text{stiff}} = 10E_{\text{soft}}$ and $\nu = 0.25$. A similar problem was considered by Miehe and Bayreuther [4]. Figure 4 illustrates the rate of convergence for the Conjugate Gradient (CG) and Generalized Minimum Residual (GMRES) iterative solvers using the two-grid preconditioner briefly outlined in Section 3. The transfer of displacements from the coarse to fine grid uses three types of transfer operators, i.e. stress (STR), modified stress (ModSTR) and

displacement (DISP). Furthermore, this is compared with the overlapping additive Schwarz preconditioner (ASM).

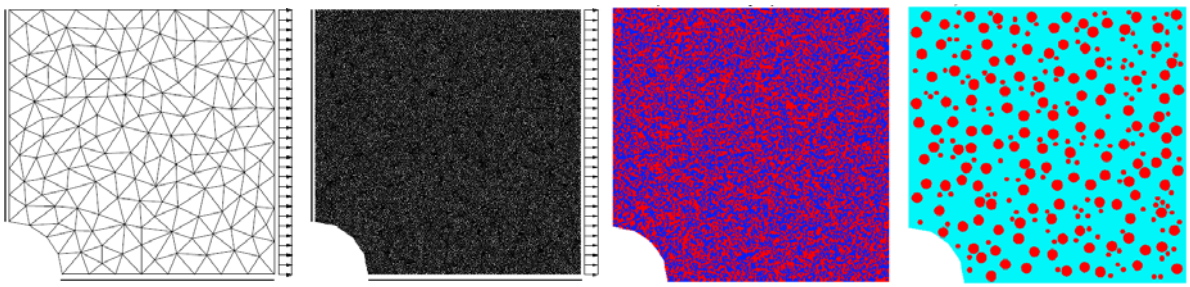

(a) (b) (c) (d)

Figure 3: Elastic heterogeneous specimen with a hole. (a) Coarse mesh, (b) fine mesh, (c) randomly distributed heterogenities (d) randomly distributed fibres.

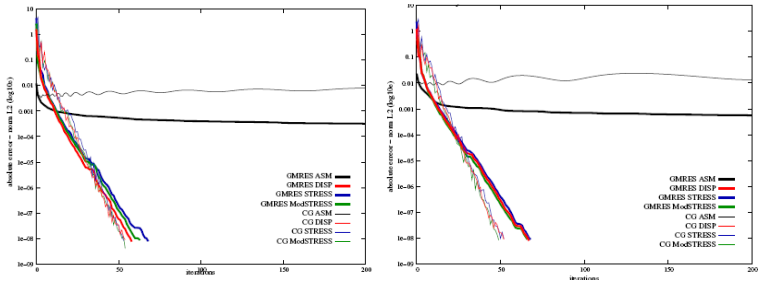

Figure 4: Convergence rate iterative solvers.

It is clear that, compared to the ASM preconditioner (which in the case of CG does not converge), the two-grid preconditioner is very effective for both CG and GMRES, for all the transfer operators.

Acknowledgement

The authors gratefully acknowledge the support of the UK Engineering and Physical Sciences Research Council (Grant Ref: EP/D500273).

References

[1] Kouznetsova VG. Computational homogenization for the multi-scale analysis of multi-phase materials, PhD, Technische Universiteit, Eindhoven, 2002.

[2] Kaczmarczyk L, Pearce CJ and Bicanic N. Scale transition and enforcement of RVE boundary conditions in second-order computational homogenization, *Int. J. Numer. Meth. Engng* 2008; 74:506-522

[3] Larsson R and Diebels S. A second-order homogenization procedure for multi-scale analysis based on micropolar kinematics. *Int. J. Numer. Meth. Engng* 2007; 69:2485-2512.

[4] Miehe C and Bayreuther CG. On multiscale FE analyses of heterogeneous structures: From homogenization to multigrid solvers, *Int. J. Numer. Meth. Engng* 2007; 71:1135-1180.

[5] Kaczmarczyk L and Pearce CJ. A corotational hybrid-Trefftz stress formulation for modelling cohesive cracks. *Submitted to Comput. Methods Appl. Mech. Engrg*.

[6] Teixeira de Freitas JA. Formulation of elastostatic hybrid-Trefftz stress elements, *Comput. Methods Appl. Mech. Engrg* 1998; 153:127-151.

[7] Kok-Kwang Phoon, et al. Fast iterative solution of large undrained soil structure interaction problems. Int. J. Numer. Anal. Meth. Geomech 2003; 27:159-181.

[8] Kasparek EM. An efficient triangular plate element with C1-continuity. *Int. J. Numer. Meth. Engng*. 2007; 73:1010 – 1026.

Proceedings of the 6th International Conference on
Computation of Shell and Spatial Structures
IASS-IACM 2008: "Spanning Nano to Mega"
28-31 May 2008, Cornell University, Ithaca, NY, USA
John F. ABEL and J. Robert COOKE (eds.)

Analysis of thin layer ductile concrete as a seismic retrofit for masonry infill walls

Marios A. KYRIAKIDES, Sarah L. BILLINGTON*

* Associate Professor, Dept. of Civil & Environmental Engineering
Yang & Yamazaki Environmental & Energy Bldg, Room 285A
473 Via Ortega, Stanford University, Stanford, CA 94305-4020
Email: billington@stanford.edu

Abstract

A thin layer of ductile concrete has been experimentally investigated as a seismic retrofit for unreinforced masonry infill walls in non-ductile reinforced concrete frames. Different modeling approaches available in a commercial finite-element code are performed to predict the performance of retrofitted masonry infilled non-ductile concrete structures under monotonic and cyclic loading. The aim of the research is to develop reliable methodologies for assessing the performance of such structures using nonlinear finite-element analysis, to be used by researchers and practitioners.

1. Introduction

Recent earthquakes have demonstrated the vulnerability of masonry infilled reinforced concrete frame structures (e.g., 1999 Kocaeli, 2003 Boumerdes). A new retrofit technique specifically for unreinforced masonry infills in non-ductile reinforced concrete frames is currently under investigation. The technique uses a sprayable, ductile fiber-reinforced mortar material referred to as Engineered Cementitious Composites, or ECC, which is applied as a thin layer to unreinforced masonry walls. The aim is to develop a cost-effective retrofit technique that will improve the seismic performance of the frame-infill system by enhancing its ductility and delaying its strength degradation. The use of a spray-on ECC layer is proposed to tie the masonry wall together as it is undergoing cyclic lateral loads and avoid shear failure in the columns of the bounding frame. Furthermore, by tying the ECC to the beams above and below the wall an alternate shear path is provided for the lateral load through the wall rather than having the load shed to the columns after the wall is damaged, thus causing a brittle failure.

Compression and flexural tests of masonry specimens with various retrofits using thin layers of ECC have been performed and small scale in-plane wall tests have been conducted to validate the proposed retrofit technique (final test to be completed in April 2008).

A major goal of the project is to compare modeling techniques across software platforms for detailed nonlinear finite element analyses of infill frame performance. We will present the initial computational work performed at Stanford in comparison to the results of our collaborators (Prof. K. Willam at U. Colorado Boulder and Prof. P. Shing at UC-San Deigo). At Stanford we are using the software DIANA and we are performing 2D analyses under monotonic and cyclic loading with constitutive models developed specifically for ECC in combination with various strategies for modeling concrete and masonry. The failure modes to model include multiple cracking and tensile strain hardening in the ECC, diagonal cracking and bed joint sliding in masonry, flexural hinging in frame columns, shear failure in beam-column joints and tensile failure in frame columns (due to wall-frame "rocking"). All of these failure modes have occurred in one or more of the wall tests performed to date.

The developed models will be used to predict large-scale performance of a two-thirds-scale model of a two-bay three-story infilled frame to be tested on the shake table at the UC-San Diego in late 2008. Simplified design and analysis tools for practitioners will then be developed.

2. Experimental investigation of ECC as a retrofit

The ductile cement-based composite under investigation is a class of high performance fiber-reinforced cement-based composites referred to as Engineered Cementitious Composites (ECC). In particular, a sprayable version of this material was recently reported and was capable of being sprayed on to a concrete wall achieving a thickness of 45mm (Kim et al. [2]). The mix design consists of Type I Portland cement, class F fly ash, calcium aluminate cement, fine silica sand and 2% by volume of short, chopped polyvinyl alcohol fibers that have been treated with oil.

2.1 Small scale tests

Small scale tests have been conducted using different retrofit techniques in order to validate the performance of ECC when applied on a masonry wall. The aim of these tests was to investigate the impact of a 13mm layer of ECC on plain masonry specimens in terms of changes in stiffness, strength and ductility as well as to study the bond between the ECC layer and the brick surface.

Compression tests have shown that when a thin layer of ECC is applied to a plain masonry prism, the strength and stiffness are increased by ~45% and ~60% respectively compared to those of a plain specimen. Moreover, surface preparation is important in order to improve the bond between the retrofit and the brick surface and avoid delamination. Small dowels used to tie the ECC to the prisms improved the bond between the ECC and the masonry; however these dowels also reduced the compressive strength of the specimen by damaging the brick during installation.

Flexural tests have indicated that the strength and more importantly the ductility of a retrofitted brick beam under four-point bending are increased tremendously. Especially when the thin layer of ECC is slightly reinforced, more cracks are developed and propagate in the constant moment region leading to a more ductile response. On the other hand, plain brick beams demonstrated very brittle failure with approximately 20-25 times lower strength.

Triplet tests were conducted wherein three bricks were joined by ECC in the joint and tested in shear (loading the central brick while supporting the outer bricks) to evaluate the shear strength of the ECC-brick bond. It was found that the bond between the ECC layer and the brick surface was similar to that of plain mortar and brick measuring on average 345kPa and exhibiting a clean delamination. When bonding agent was applied, the bond was substantially enhanced to 2070kPa and delamination was not observed.

2.2 In-plane wall tests

Small scale in-plane wall tests – approximately $1/5^{th}$ scale – with details typical of 1920s construction in the United States have been conducted. The aim of this group of tests was to get a first validation of the retrofit technique through the interaction between the retrofitted masonry infill and the bounding non-ductile reinforced concrete frame. Three wall tests have been tested to date at Stanford University. The fourth and final specimen will be tested in April, 2008. The three tested specimens have captured the anticipated target responses of (1) failure of the masonry infill leading to failure of the bounding frame (control specimen) (2) eliminating failure of the masonry infill and instead have failure of the bounding frame and (3) eliminating failure of the masonry infill and preventing shear failure of the bounding frame.

The test set-up as well as the response of the unretrofitted specimen (control specimen) compared to the response of specimen 3 (retrofitted specimen) are shown in Figure 1. Specimen 3 was retrofitted with a 13mm layer of ECC reinforced with 0.4% welded wire fabric (WWF). Strips of bonding agent were painted on the masonry surface to improve the bond between the ECC layer and the brick surface. Shear dowels were initially placed at the top concrete beam and bottom concrete base and then covered by the ECC layer, creating an alternate path for lateral load from the frame into the wall. As shown in Figure 1(b), higher lateral strength was reached compared to the unretrofitted specimen with a gradual drop of the lateral strength to 60-68% of the peak at 3.5% drift. Tensile cracks at the columns occurred at early drift levels leading to a “rocking” motion of the infilled concrete frame.

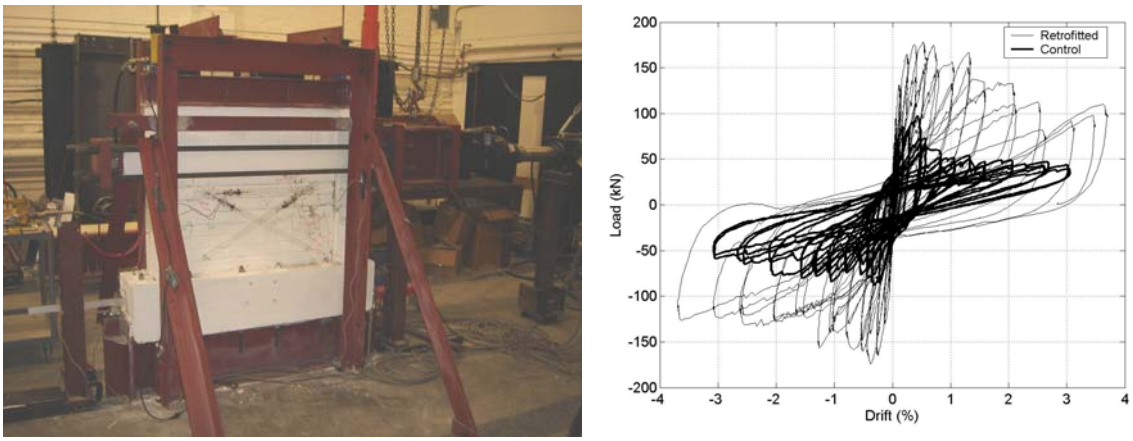

(a) (b)

Figure 1: Test set-up (a) and response of two masonry infilled frames (b) tested at Stanford University.

3. Analytical investigation of retrofitted walls

The ability to predict adequately the performance of a masonry infilled reinforced concrete structure has been a significant area of research over the last several decades in large part due to its importance for practitioners. This effort becomes more complicated when a retrofit technique is applied on the masonry infill. We are exploring the ability of state-of-the-art nonlinear finite element analysis methods incorporating existing and new constitutive models to predict the performance of such structures.

3.1 Concrete model selection: analysis of a bare concrete frame

A series of analyses of a bare concrete frame tested by Mehrabi et al.[4] has been conducted in order to examine different concrete modeling approaches. The bare frame modeled was a ½-scale model of the interior frame located at the bottom of a six-story, three bay office building. The frame was designed to satisfy the ACI 318-89 (1989) provisions and the design loads complied with the specifications of the Uniform Building Code (UBC) (1991). The specimen was loaded monotonically. Flexural cracks initiated at the bottom sections of both columns, followed by shear cracks in the beam-to-column joints and finally concrete crashing was observed at the upper end of the east column and lower end of the west column. 8-noded quadrilateral plane stress elements have been used to model the concrete frame following a linear softening model in tension and a parabolic model

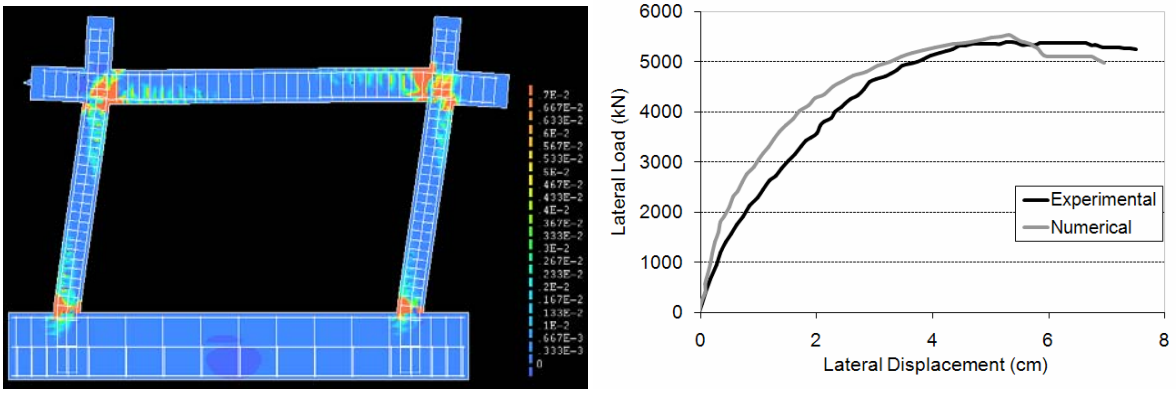

(a) (b)

Figure 2: Principal tensile strains (a) and experimental (Mehrabi et al.[4]) vs numerical load-displacement response of a reinforced concrete bare frame.

in compression. The reinforcement was model as embedded bar elements following the Von Mises yield condition with strain hardening. Figure 2 shows (a) the principal tensile strains obtained by the analytical model and (b) the analytical vs. experimental load-displacement response of a reinforced concrete bare frame. Figure 2(a) indicates that large values of principal tensile strains occur at the base of the columns and at the beam-column joints, locations where all major cracks formed during the test. Figure 2(b) also shows that the modeling approach captures the peak load and the failure modes reasonably well. However, the initial stiffness is not as well captured.

3.2 Masonry modeling: with and without an ECC retrofit.

3.2.1 Small scale masonry component tests

The small scale masonry component tests conducted with a thin layer of ECC are being used for the initial validation of the analytical models. 2D finite-element analyses are being performed. Plane stress elements are being used to model the brick units with both smeared crack and discrete crack modeling approaches being studied to capture brick cracking behavior. Interface elements are introduced between the brick units to represent the mortar joints to capture crack formation and shear deformation in these joints. Plane stress elements and a constitutive model developed for ECC (Han et. al [1]) are used to simulate the thin retrofit applied on the flexural brick beams. This model uses a multi-linear function in both compression and tension and has a polynomial unloading curve with more energy dissipation than traditional concrete, a unique characteristic of ECC. A schematic of the retrofitted brick beam tested in flexure and the brick-mortar-ECC finite element modeling approach is shown in Figure 3.

(a) (b)

Figure 3: (a) Flexural test set-up of an ECC-retrofitted brick beam, and (b) brick-mortar-ECC finite element modeling approach.

3.2.3 In-plane wall tests

Analyses of the in-plane wall tests (retrofitted and unretrofitted) are being conducted in order to capture the failure mechanisms obtained from the tests. Different modeling approaches are being investigated for both the modeling of the concrete frame under cycling load (Kwan and Billington [3]) and for the modeling of the masonry infill (Rots [5]). However, the main difference in this group of analyses compared to the analyses conducted for the flexural brick beams is the application of the ECC plane stress elements. The ability to apply ECC plane stress elements on existing brick plane stress elements (i.e. an overlay) in 2D modeling is being investigated.

Results of the finite-element analyses will be presented during the conference.

Acknowledgements

This research is sponsored by a grant from the National Science Foundation (NSF-NEESR Grant No. 0530737). The authors thank Soares Masonry Inc. for the donation of building the infill walls as well as Williams Form, Kuraray Co. Ltd., U.S. Silica Company, Salt River Materials Group, Univar USA Inc., and LaFarge for additional material donations. Collaboration and input from Professors Benson Shing and Kaspar Willam as well as the advisory panel of Joseph Maffei Greg Kingsley, Dave Brieholtz, John Kariotis, Ron Mayes, Paul Murray and Mike Valley are gratefully acknowledged. Finite element modeling is performed using the DIANA v9.1 finite element software.

References

[1] Han, T. S., Feenstra, P. H. and Billington, S.L. (2003), "Simulation of Highly Ductile Fiber-Reinforced Cement-Based Composites." *ACI Structural Journal*, 100(6), pp. 749-757.

[2] Kim, Y.Y., Kong, H.J., and Li, V.C. (2003), "Design of Engineered Cementitious Composite (ECC) Suitable for Wet-Mixture Shotcreting." *ACI Materials Journal*, 100(6), pp. 511-518.

[3] Kwan, W.P. and Billington, S.L. (2001), "Simulation of Structural Concrete under Cyclic Load." *Journal of Structural Engineering*, ASCE, 127(12), pp. 1391-1401.

[4] Mehrabi, A.B., Shing, P.B., Schuller, M.P., and Noland, J.L. (1994). "Performance of Masonry-Infilled R/C Frames under In-Plane Lateral Loads." *Report No. CU/SR-94-6*, Dept. of Civil, Environmental, and Architectural Engineering, University of Colorado, Boulder, CO.

[5] Rots, J.G., (1997) "Structural Masonry. An Experimental /Numerical Basis for Practical Design Rules." TNO Building and Construction Research, Rijswijk, Netherlands.

Proceedings of the 6th International Conference on
Computation of Shell and Spatial Structures
IASS-IACM 2008: "Spanning Nano to Mega"
28-31 May 2008, Cornell University, Ithaca, NY, USA
John F. ABEL and J. Robert COOKE (eds.)

Mesoscopic failure simulation of concrete and life-cycle computation of concrete structures

Kohei NAGAI*, Koich MAEKAWA

*Department of Civil Engineering, University of Tokyo
7-3-1, Hongo, Bunkyo-ku Tokyo 113-8656 JAPAN
nagai@concrete.t.u-tokyo.ac.jp

Abstract

This paper describes two approaches to develop an analytical scheme for a prediction of life span of concrete structure. Failure simulation of concrete at material scale by discrete analysis method, which can consider the effect of its component including environmental effect, is conducted to evaluate the concrete mechanical damage or fracture directly. Second approach at structural level is by FEM based scheme that challenges to predict a behavior of concrete structure on long term where a durability mechanics (fatigue, creep, shrinkage, thermal effect etc.) occupies a central role. Life-cycle computation of RC slab with developed material constitutive model is carried out and verified.

1. Introduction

Due to the fact that concrete structures deteriorate with time by various factors, e.g. environments, service load and earthquake and so on, methodologies of durability-based design and strategic maintenance for the concrete structures are necessary to be developed. A computational scheme is required for a prediction of structural life cycle performance with knowledge on short and long term material and structural behaviors that is indispensable to achieve it. To evaluate the mechanical behaviors of concrete at material level, a mesoscopic simulation, where concrete is treated as heterogeneous material, can be an efficient tool. Since the composing materials themselves are modeled in the analyzed concrete, it is possible to consider the mechanical properties of each component and interface between the components to which the deterioration mechanism can be introduced. Rigid Body Spring Model (RBSM), one of the discrete analysis methods, is adopted in this study for the simulation of concrete failure. Fracture and failure behaviors of concrete in compression and tension were predicted and discussed. The outcome obtained from the research at meso or material scale will be useful for development of space averaged constitutive model for FEM based simulation platform of the life-cycle performance of concrete structures. The durability mechanics tool based on the multi-directional fixed crack model for RC developed by Maekawa *et al.*, in which the material constitutive models are formulated with micro mechanics and chemo-physics has been extended in recent years for high cyclic loading with direct path integration scheme. The applicability of the developed path-integral scheme was verified for the structural fatigue analysis of RC beams and slabs under fixed pulsating and moving load schemes.

2. Mesoscopic failure simulation of concrete

Concrete is a heterogeneous material consisting of mortar and aggregate at meso level. Evaluation of the fracture process at this level is useful to clarify the material characteristic of concrete. However, the analytical approach at this level has not yet been sufficiently investigated. The Authors have conducted the two- and three-dimensional mesoscopic analysis of failure of concrete by Rigid Body Spring Model (RBSM) over the past few years (Nagai *et al.* [8][9]).

The RBSM developed by Kawai [1] is one of discrete numerical analysis method. Analytical model is divided into polyhedron elements whose faces are interconnected by springs. Each element has three transitional and three rotational degrees of freedom those are given at some point inside of element. One normal and two shear

springs are placed at some point on each face. Since cracks initiate and propagate along the boundary face, the mesh arrangement may affect fracture direction. To avoid formation of cracks with a certain direction, a random geometry is introduced using a three-dimensional Voronoi diagram. The Voronoi diagram is the collection of Voronoi cells. Each cell represents mortar or aggregate element in the analysis.

Constitutive model given to the springs between elements are explained in mainly our previous research (Nagai *et al.* [9]). The normal spring in compression zone always acts elastic and never shows breakage nor softening behavior. After it reaches tensile strength, softening behavior governed by the crack width is given. For shear spring, an elasto plastic model is applied. It means that the compression failure of specimen in macro scale is presented by meso scale tensile and shear failures between elements.

Simulations of failure of concrete under uniaxial compression and tension conditions are conducted where the shape of the coarse aggregate in the concrete is circular. The analyzed specimen (70×70×140 mm) where the number of element is 39,162 including 17,082 elements of aggregate is shown in Figure 2. Average element size is 2.60 mm^3. Aggregate volume in the specimen is 30.9%. In compression test, the top and bottom boundaries of specimen are fixed in the lateral direction. In the tension test, the loading boundaries in the lateral direction are not fixed. The predicted stress-strain relationship and deformation at failure are presented in Figure 2. In compression test, natures of the predicted curves of stress-strain in axial and lateral directions are similar to the experimental results mentioned by Stock *et al.* [9]. Deformations of specimens at failure shows macro shear cracks as observed in usual experiments. The result of simulation where the loading boundary in lateral direction is not fixed is presented in the graph, in which a slight reduction in macroscopic strength due to the elimination of friction on the loading boundary is observed in the analysis, similarly to the experiment. Since the loading boundary of specimen cannot restrict the expansion of the specimen in the lateral direction, the specimen fails just after the rapid increasing of lateral strain. In tensile analysis, simulated stress-strain curve and deformation at failure, in which the localized crack is predicted, are similar to that observed in usual experiment. Based on the mesoscopic simulation scheme presented here, the environmental effect on long term is able to be introduced in the future (Ueda *et al.* [10], Wang *et al.* [11]).

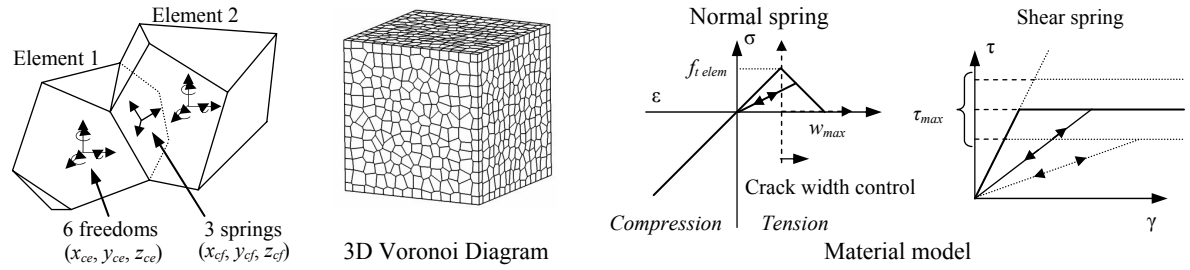

Figure1: 3D RBSM

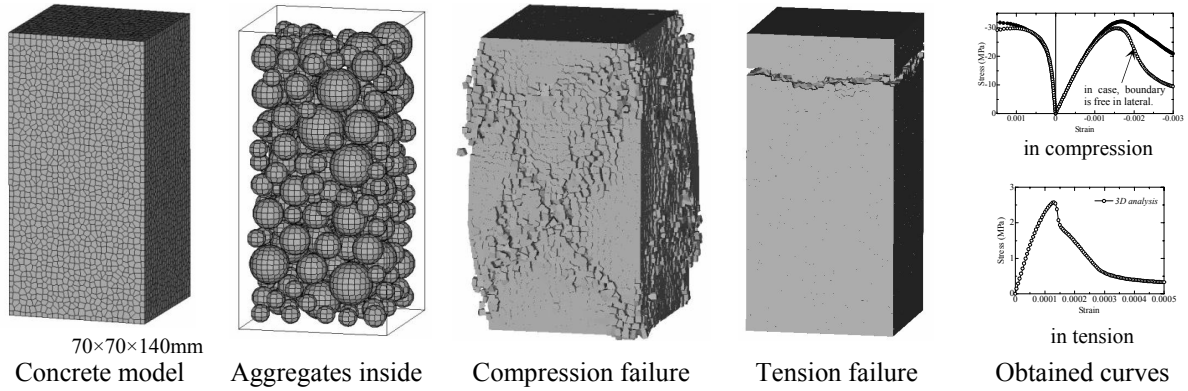

Figure 2: Compression and tension analyses of concrete model by RBSM

3. Life-cycle computation of concrete structure

To ultimately realize the explicit prediction and simulation of structural service life and safety under specified loads and ambient condition we need a rational structural mechanics platform in which mechanistic based constitutive material models are rooted. Here proposed is a multi-directional fixed crack modeling approach of RC (Figure 3) in which the interaction between cracks is taken in to account by the active crack method (Maekawa *et al.* [4]) on the smeared compression stress field.

The fatigue simulation system for RC structure proposed is based on the direct path integral scheme. Numerical simulation is conducted by tracing the evolution of microscopic material states at each moment with multi directional fixed crack model (Maekawa *et al.* [4]). This simulation system has been enhanced for fatigue analyses by using logarithmic integral method (Maekawa *et al.* [5]). Damage degradation is expressed by incremental plasticity and fracturing. The framework is made up with essential three constitutive models, compression, tension and crack shear, which treat the cumulative fatigue damaging

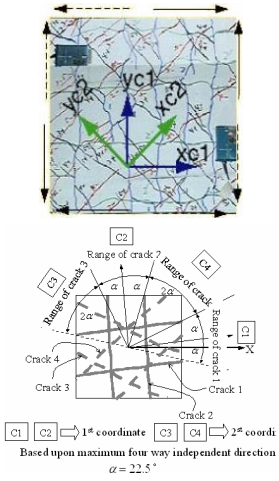

	Compression model	Tension model	Crack shear model
Core Constitutive low	Stress-strain $\sigma = E_0 K_C \varepsilon_e$ $\varepsilon = \varepsilon_e + \varepsilon_p$	Stress-strain $\sigma = E_0 K_T \varepsilon_e$ $\varepsilon = \varepsilon_e + \varepsilon_p$	Shear stress-shear strain $\tau = \int_{-\pi/2}^{\pi/2} R'_c(\omega,\delta,\theta)\sin\theta d\theta$
Enhanced model for High cycle fatigue	Fracture parameter Kc considers time dependent plasticity & fracturing and cyclic fatigue damage $dK_C = \left(\frac{\partial K_C}{\partial t}\right)dt + \left(\frac{\partial K_C}{\partial \varepsilon_e}\right)d\varepsilon_e$ (time dependent / cyclic fatigue) $\left(\frac{\partial K_C}{\partial \varepsilon_e}\right) = \lambda \sim when F_k = 0$ $\left(\frac{\partial K_C}{\partial \varepsilon_e}\right) = -\left(\frac{\partial F_k}{\partial \varepsilon_e}\right)\left(\frac{\partial F_k}{\partial K}\right) + \lambda \sim when F_k = 0$ $\lambda = K^3 \cdot (1-K^4) \cdot g \cdot R$ El-Kachif and Maekawa 2004	Fracture parameter K_T considers time dependent fracturing and cyclic fatigue damage $dK_T = Fdt + Gd\varepsilon_e + Hd\varepsilon_e$ (Time dependent fracturing / Cyclic fatigue damage) Maekawa et al. 2003, Hisasue 2005	Accumulated path function X reduce shear associated with cyclic fatigue damage $\tau = X \cdot \tau_0(\delta,\omega)$ (function / original model) $X = 1 - \frac{1}{10}\log_{10}\left\{1 + \int\left\lvert d(\delta/\omega)\right\rvert\right\} \geq 0.1$ Contact density model by Li & Maekawa 1989 Modification of accumulated path function by Gebreyouhannes 2006
Physical meaning	Decrease of stiffness and plasticity accumulation by continuous fracturing of concrete	Decrease of tension stiffness by bond fatigue	Decrease of shear transfer normal to crack by continuous deterioration of rough crack surface

Figure 3: Fatigue simulation constitutive model for RC with multi-directional cracking

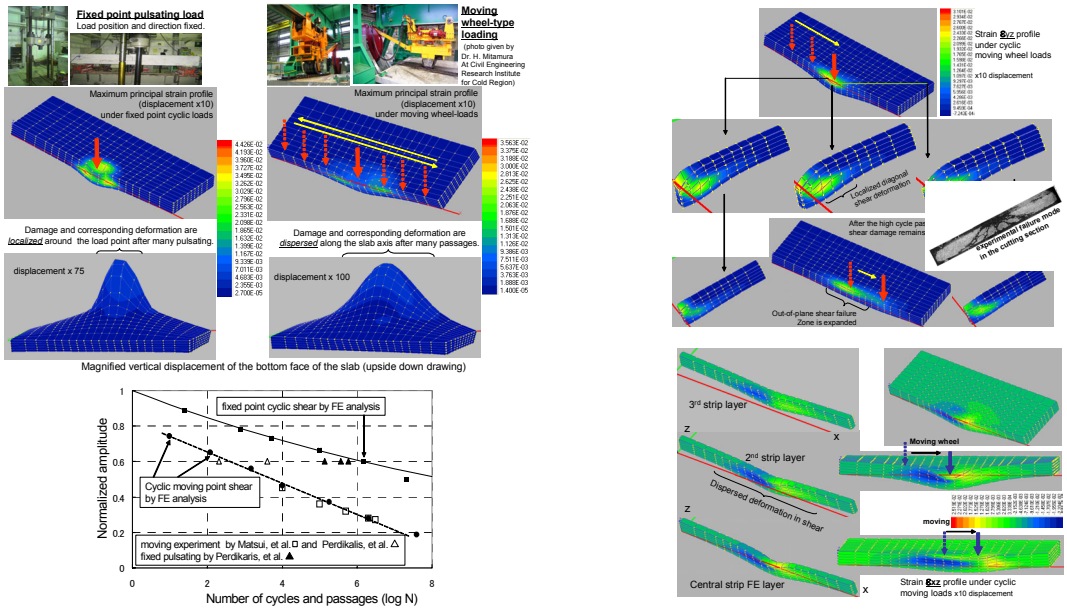

Figure 4: Simulation results for the failure mode of RC slabs under fixed point pulsation and wheel-type moving loads

and time dependency effects. Full-3D simulation system is based on these core models (Figure 3).

The fatigue life assessment of RC slabs is a key issue in the life-cycle design and maintenance of bridges. RC bridge decks are usually subjected to heavy traffic loads with high repetition of traffic passage and varying ambient conditions. Thus, the simulation of RC bridge deck slabs is appropriate for verification of the proposed computational durability mechanics platform. The direct time and strain path-integral scheme of structural reinforced concrete is coupled with the moisture migration within micro-pores and cracks (Maekawa *et al.* [3]). This computational platform is applied to the life-cycle simulation of RC slabs under fixed point pulsation and moving wheel-type loads exposed to different environmental conditions. As indicated in Figure 4, the failure mode for the fixed pulsating load is typical punching failure with conical crack planes; whereas, the wheel-type moving load passages produce highly anisotropic shear failure and extends diagonally only in the transverse direction. This peculiar difference in the failure mode for both type of loading is experimentally observed by (Matsui and Maeda [2]).

Figure 4 shows, the computed S-N diagram for both types of loading compared with experimentally observed results. The moving wheel-type fatigue loads greatly deteriorates the fatigue life, by nearly 2-3 orders lower, as compared to that of the fixed point fatigue load. This is consistent with the experimental results observed by (Matsui [6]). Moving loads create through vertical cracks transverse to the direction of moving load. Consequently, reversal of shear stress along the cracks and the interaction with shear cracks are thought to play governing role for the reduced fatigue life of RC slabs. The active crack method plays a central role in dealing with the multi-directional cracks generated by the moving loads. The fact that physically reasonable results have been achieved is attributed to the rationale in structural mechanics and realistic nature of the constitutive material models.

Conclusion

The two approach presented here will be unified organically in the future by the way of that the obtained result at meso scale is incorporated into the space averaged constitutive model for RC analysis at structural scale.

References

[1] Kawai T New discrete models and their application to seismic response analysis of structure. *Nuclear Engineering and Design*, 1978; 48; 207-229.

[2] Maeda Y and Matsui S Fatigue of reinforced concrete slabs under trucking wheel load. *Proceedings of JCI,* 1984; 6; 221-224.

[3] Maekawa K, Gebreyouhannes E, Mishima T and X An Three-dimensional fatigue simulation of RC slabs under traveling wheel-type loads. *Journal of Advanced Concrete Technology*, 2006; 4(3); 445-457.

[4] Maekawa K, Pimanmas A, and Okamura H. Nonlinear Mechanics of Reinforced Concrete. Spon Press, London, 2003.

[5] Maekawa K, Toongoenthong K, Gebreyouhannes E and Kishi T Direct path-integral scheme for fatigue simulation of reinforced concrete in shear. *Journal of Advanced Concrete Technology*, 2006; 4(1); 159-177.

[6] Matsui S Fatigue strength of RC-slabs of highway bridge by wheel running machine and influence of water on fatigue. *Proceedings of Japan Concrete Institute*, 1987; 9; 2; 627-632.

[7] Nagai K, Sato Y and Ueda T Mesoscopic simulation of failure of mortar and concrete by 2D RBSM. *Journal of Advanced Concrete Technology*, 2004; 2(3); 359-374.

[8] Nagai K, Sato Y and Ueda T Mesoscopic simulation of failure of mortar and concrete by 3D RBSM. *Journal of Advanced Concrete Technology*, 2005; 3(3); 385-402.

[9] Stock AF, Hannant DJ and Williams RIT The effect of aggregate concentration upon the strength and modulus of elasticity of concrete. *Magazine of Concrete Research*, 1979; 31 (109); 225-234.

[10] Ueda T, Hasan M, Nagai K and Sato Y Stress-strain relationship of concrete damaged by freezing and thawing cycles, *Proceeding of FraMCos-5*; 2004: 2; 645-652.

[11] Wang L, Soda M, Ueda T Simulation of Chloride diffusivity of cracked concrete based on RBSM and truss network model, *Journal of Advanced Concrete Technology*, 2008; 6(1); 143-155.